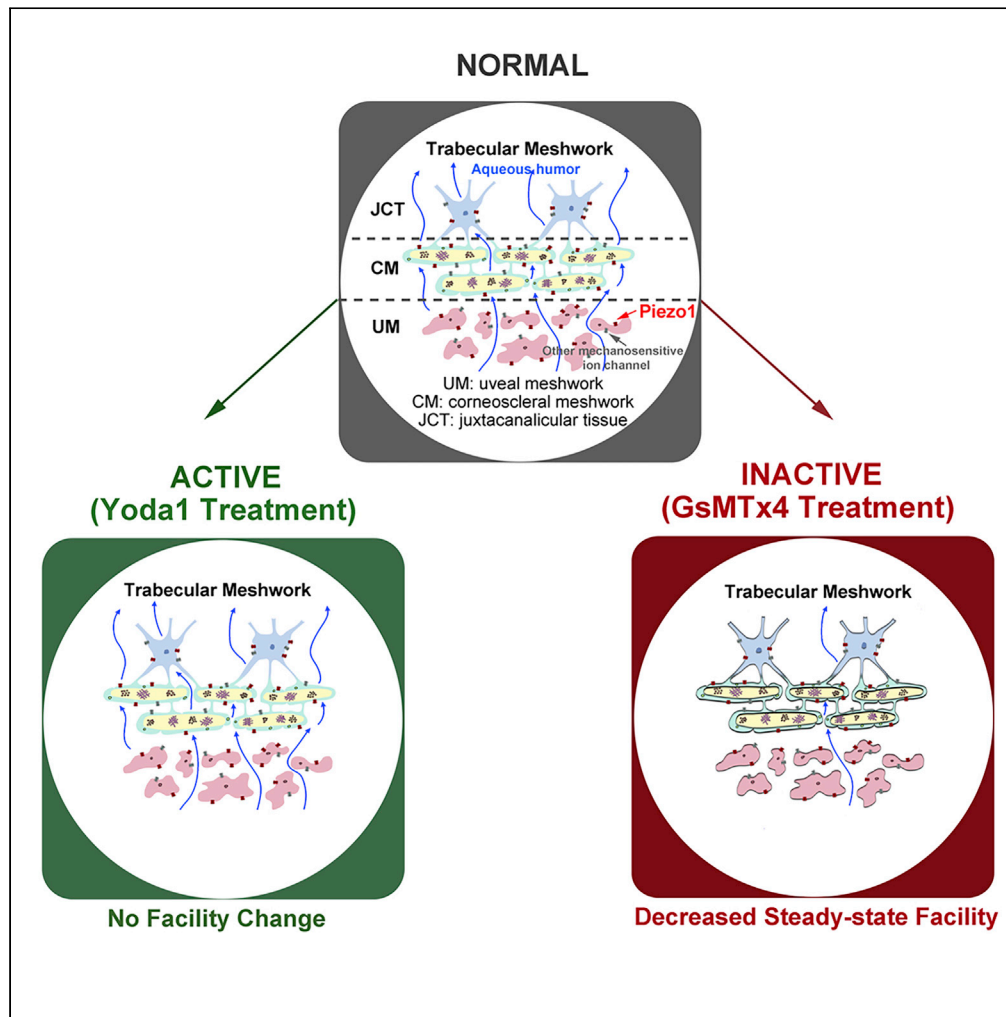**Article**

The role of Piezo1 in conventional aqueous humor outflow dynamics

Wei Zhu, Fei Hou, Jingwang Fang, ..., Ningli Wang, C. Ross Ethier, KeWei Wang

wzhu@qdu.edu.cn (W.Z.)
wangkw@qdu.edu.cn (K.W.)

HIGHLIGHTS

Piezo1 is functionally expressed in the TM, the most important tissue controlling IOP

Suppression of mechanosensitive channel leads to a significant decrease in facility

Our data suggest a role for Piezo in pathological situations and rapid IOP transients

Article

The role of Piezo1 in conventional aqueous humor outflow dynamics

Wei Zhu,[1,2,10,11,*] Fei Hou,[1,4,10] Jingwang Fang,[1,10] Mohammad Reza Bahrani Fard,[3] Yani Liu,[1] Shouyan Ren,[4] Shen Wu,[5] Yunkun Qi,[1] Shangru Sui,[1] A. Thomas Read,[3] Joseph M. Sherwood,[6] Wei Zou,[7] Hongxia Yu,[1] Jingxue Zhang,[5] Darryl R. Overby,[6] Ningli Wang,[5] C. Ross Ethier,[3,8] and KeWei Wang[1,9,*]

SUMMARY

Controlling intraocular pressure (IOP) remains the mainstay of glaucoma therapy. The trabecular meshwork (TM), the key tissue responsible for aqueous humor (AH) outflow and IOP maintenance, is very sensitive to mechanical forces. However, it is not understood whether Piezo channels, very sensitive mechanosensors, functionally influence AH outflow. Here, we characterize the role of Piezo1 in conventional AH outflow. Immunostaining and western blot analysis showed that Piezo1 is widely expressed by TM. Patch-clamp recordings in TM cells confirmed the activation of Piezo1-derived mechanosensitive currents. Importantly, the antagonist GsMTx4 for mechanosensitive channels significantly decreased steady-state facility, yet activation of Piezo1 by the specific agonist Yoda1 did not lead to a facility change. Furthermore, GsMTx4, but not Yoda1, caused a significant increase in ocular compliance, a measure of the eye's transient response to IOP perturbation. Our findings demonstrate a potential role for Piezo1 in conventional outflow, likely under pathological and rapid transient conditions.

INTRODUCTION

Ocular health requires a stable, suitable level of intraocular pressure (IOP), which is determined by the rate of production of aqueous humor (AH) and its resistance to drainage from the eye (Chandler, 1977). Increased resistance to AH outflow leads to a sustained elevation of IOP, which is the major risk factor for glaucomatous optic neuropathy (Buckingham et al., 2008; Goel et al., 2010) and its attendant vision loss (Sihota et al., 2018).

The conventional AH outflow pathway, including the trabecular meshwork (TM) and Schlemm canal (SC), drains the majority of AH in humans (Weinreb et al., 2014). The TM contributes 50%–75% of the resistance to AH outflow in the conventional outflow pathway (Goel et al., 2010). It is mechanosensitive (Liton and Gonzalez, 2008; Ramos et al., 2009), and improved understanding of mechanotransduction pathways in this tissue would enable novel strategies for controlling IOP and improving glaucoma therapy. However, it is still poorly understood how the TM senses and responds to mechanical forces. Recently, mechanosensitive ion channels have been reported in the TM (Tran et al., 2014; Yarishkin et al., 2019). Specifically, TRPV4 (transient receptor potential cation channel subfamily V member 4) and TREK-1 (TWIK-related potassium channel-1) were shown to respond to mechanical force and to influence TM function by modulating calcium homeostasis, remodeling TM cell cytoskeleton, and changing TM extracellular matrix composition (Carreon et al., 2017; Ryskamp et al., 2016; Yarishkin et al., 2018).

Piezo ion channels have essential roles in transducing mechanical forces and, when compared with TRPV4 and TREK-1, are more sensitive to certain mechanical stimuli (Coste et al., 2010). For example, Piezo1, as a blood flow sensor, is required for vascular development and blood pressure regulation (Li et al., 2014; Ranade et al., 2014a; Retailleau et al., 2015). Piezo1 also has important roles in regulating the volume of red blood cells (Cahalan et al., 2015), homeostasis of epithelial cell numbers (Eisenhoffer et al., 2012), cell migration, mechanotransduction in cartilage (Lee et al., 2014), control of urinary osmolarity (Martins

[1]Department of Pharmacology, School of Pharmacy, Qingdao University, Qingdao University Medical College, 38 Dengzhou Road, Qingdao 266021, Shandong, China

[2]Beijing Advanced Innovation Center for Big Data-Based Precision Medicine, Beihang University & Capital Medical University, Beijing 100730, China

[3]George W. Woodruff School of Mechanical Engineering, Georgia Institute of Technology, Atlanta 30332, GA, USA

[4]Department of Pharmacy, Affiliated Hospital of Qingdao University, Qingdao 266003, China

[5]Beijing Institute of Ophthalmology, Beijing Tongren Hospital Eye Center, Beijing 100730 China

[6]Department of Bioengineering, Imperial College London, London, UK

[7]School of Mechatronic Engineering, Jiangsu Normal University, Xuzhou 221116, China

[8]Department of Biomedical Engineering, Georgia Institute of Technology and Emory University, Atlanta, 30332, GA, United States

[9]Institute of Innovative Drugs, Qingdao University, 38 Dengzhou Road, Qingdao 266021, Shandong, China

[10]These authors contributed equally

[11]Lead contact

*Correspondence:
wzhu@qdu.edu.cn (W.Z.),
wangkw@qdu.edu.cn (K.W.)

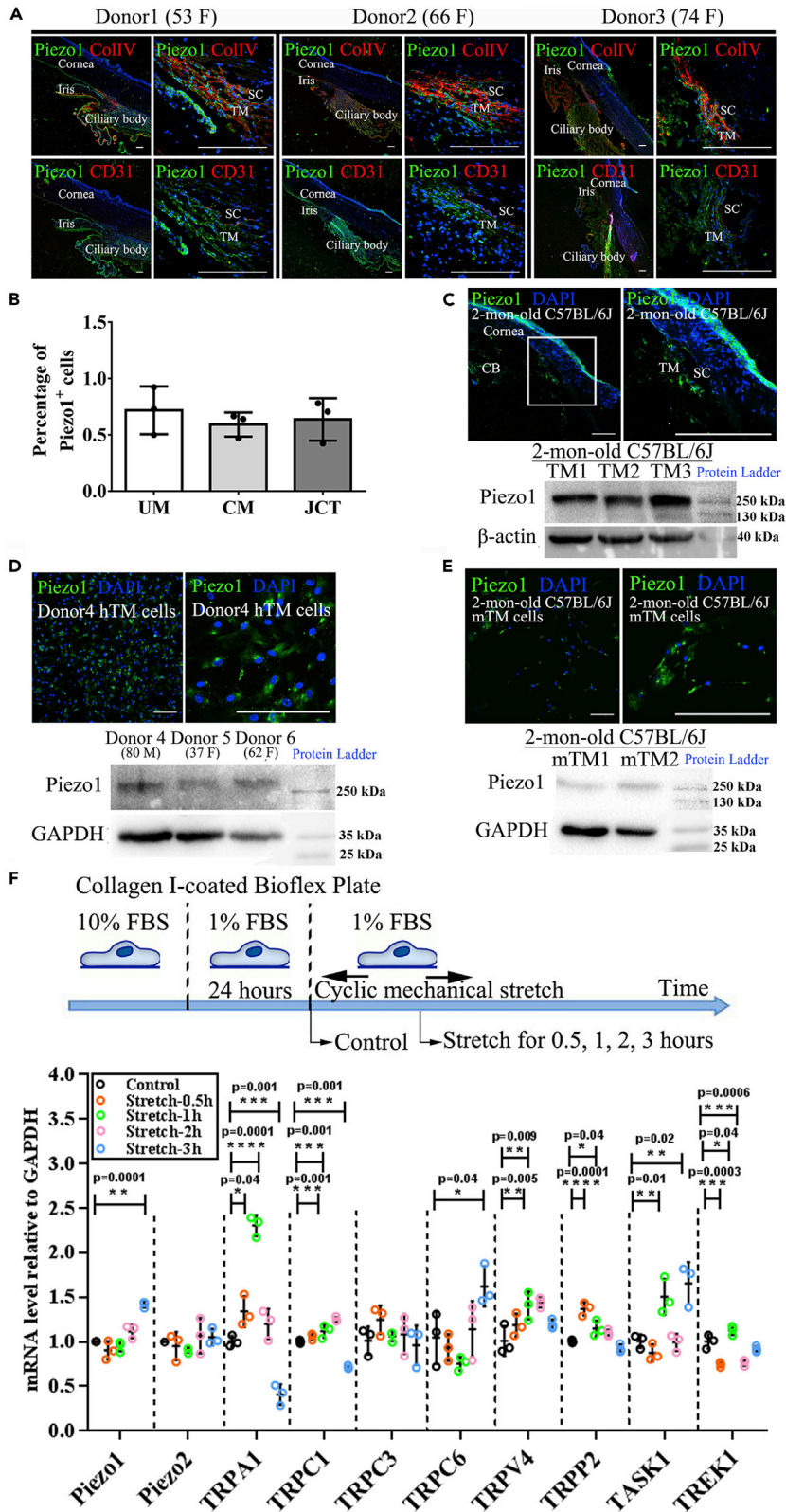https://doi.org/10.1016/j.isci.2021.102042

Figure 1. Expression of mechanosensitive ion channels in human and mouse trabecular meshwork

(A) Co-immunohistochemical (IHC) staining of Piezo1 (green) and ColIV (red, antibody labels basement membrane collagen in TM) or CD31 (red, antibody labels Schlemm canal endothelial cells). Typical results from n = 3 human eyes are shown.

(B) Quantification of percentage of cells expressing Piezo1 in subregions of the human TM, namely, the uveal meshwork (UM), the corneoscleral meshwork (CM), and the juxtacanalicular tissue (JCT).

(C) Upper panel: Piezo1 was visualized (green) in the TM of 2-month-old C57BL/6J mice. The region in the white frame is shown in magnified view at the right. Lower panel: The expression of Piezo1 in the iridocorneal angle was determined by western blot (n = 3).

(D) Piezo1 (green) in human primary TM cells was assessed by IHC staining (upper panel) and western blot (lower panel) (n = 3).

(E) Piezo1 was detected in mouse primary TM cells through IHC (green; upper panel) and western blot (lower panel) (n = 2). Nuclei were stained with DAPI (blue). Scale bars, 100 μm.

(F) Upper panel: Protocol for cyclic mechanical stretch. Lower panel: Increased expression of Piezo1 and TRP was detected in human primary TM cells subjected to cyclic mechanical stretch (n = 3). Horizontal lines indicate means; bars are standard deviation. *p < 0.05, **p < 0.01, ***p < 0.001, ****p < 0.0001 by one-way ANOVA.

et al., 2016), neural stem cell fate (Pathak et al., 2014), and neuronal axon growth (Koser et al., 2016). Piezo2 acts as a key mechanotransducer in response to gentle touch on the skin (Ikeda et al., 2014; Ranade et al., 2014b; Woo et al., 2014), proprioception (Woo et al., 2015), and airway stretch and lung inflation (Nonomura et al., 2017). Genetic gain or loss of Piezo channel function is associated with several diseases such as hereditary xerocytosis (Lukacs et al., 2015), allodynia (Eijkelkamp et al., 2013), and distal arthrogryposis (Coste et al., 2013). However, it remains unknown whether Piezo channels can sense mechanical stimuli in the TM and whether they have a role in regulating AH outflow.

The goal of the present study was to investigate whether and how Piezo ion channels function in AH outflow. We first confirmed the functional expression of Piezo1 in the TM by examining protein expression and cellular electrophysiology. We then determined the role of Piezo1 in the steady-state outflow of AH from the eye.

RESULTS

Piezo1 is widely expressed in human and mouse iridocorneal angle tissues

The conventional AH drainage tissues largely control IOP and are subjected to significant mechanical deformations. We therefore interrogated these tissues to determine Piezo1 expression levels and distribution. Co-immunohistochemical (IHC) staining of anterior segments from three human donors revealed that Piezo1 was robustly expressed throughout the entire TM, with positive labeling observed in 72% of cells in the uveal meshwork, 59% of cells in the corneoscleral meshwork, and 64% of cells in the juxtacanalicular tissue (Figures 1A and 1B). We also examined Piezo1 expression in mouse TM tissue, which is composed of three to four trabecular beams in the anterior meshwork (Smith et al., 2001). Positive staining of Piezo1 could also be observed throughout the mouse TM (Figure 1C). Western blot analysis confirmed the expression of Piezo1 in mouse iridocorneal angle tissues (Figure 1C). Moreover, the expression of Piezo1 was confirmed in human (Figure 1D) and mouse (Figure 1E) cultured primary TM cells by IHC and western blot.

The endothelial cells of SC adjacent to the TM are also mechanosensitive and participate in conventional aqueous outflow (Stamer et al., 2015). Co-IHC staining indicated that Piezo1 expression co-localized with the SC endothelial cell biomarker CD31 in human tissues (Figure 1A). Furthermore, Piezo1 was detected in the ciliary muscle (Figure 1A) and non-pigmented epithelial cells of the ciliary body (Figure S1), which are crucial for the regulation of unconventional outflow and AH secretion, respectively. Furthermore, strong expression of Piezo1 was detected in cornea (Figure 1). The widespread expression of Piezo1 in outflow tissues suggests that Piezo1 may play a role in modulating AH dynamics in response to mechanical stresses.

Cyclic mechanical stretch increases Piezo1 expression in TM cells

The TM undergoes significant cyclic mechanical stretching due to the ocular pulse and other perturbations (Johnstone, 2004). We therefore asked whether Piezo1 present in TM cells was functionally involved in mechanotransduction in response to such stretching. We subjected cultured human primary TM cells (Ramos et al., 2009) to cyclic mechanical stretch with an amplitude of 20% at a frequency of 1 Hz, an experimental model that mimics acute sustained elevation of IOP (Hirt and Liton, 2017; Kerr et al., 2003), and assessed
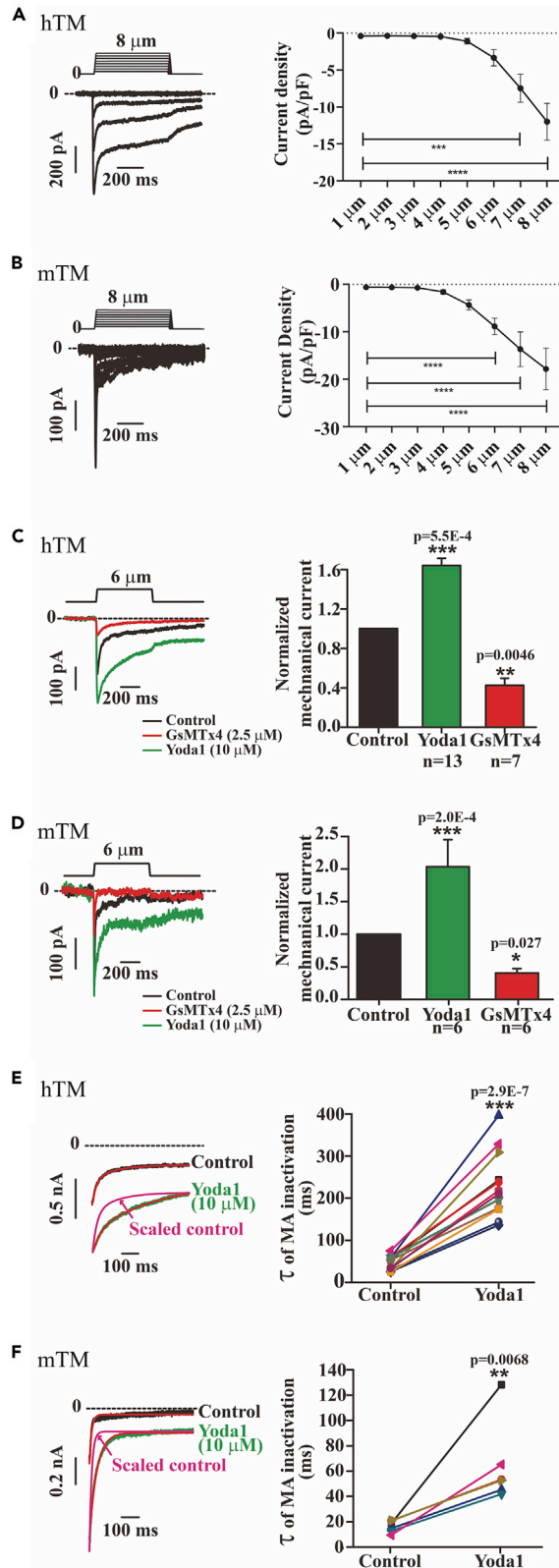
A hTM

B mTM

C hTM

D mTM

E hTM

F mTM

Figure 2. Mechanical activation of Piezo1 current in human and mouse primary TM cells

(A) Cells were subjected to a series of mechanical stimuli consisting of sequential 1 μm indentations. Representative mechanosensitive inward currents recorded in hTM cells are shown (n=13-15 cells, ***p < 0.001, ****p < 0.0001, by two-tailed t test). (B) Representative mechanosensitive inward currents recorded in mTM cells are shown (n=6-21 cells, ****p < 0.0001, by two-tailed t-test). (C) Left panels show representative mechanosensitive inward currents elicited by 6 μm mechanical stimulation in control hTM cells (black), hTM cells treated with 10 μM Yoda1 (green), or hTM cells treated with 2.5 μM GsMTx4 (red). Right panels show quantification of normalized mechanosensitive currents in the presence of Yoda1 or GsMTx4 (n=7-13 cells, ***p< 0.001, **p< 0.01, by two-tailed t-test). (D) Similar to (C), showing representative mechanosensitve inward currents in mTM cells treating with Yoda1 or GsMTx4 (n=7-13 cells, ***p < 0.001, *p < 0.05, by two-tailed t-test). (E) Left panels show inactivation current traces following 6 μm mechanical stimulation in the absence (black) or presence (green) of Yoda1 in hTM cells. Right panels show time constants of mechanically-activated current inactivation in control or Yoda1 treated cells (n=6-12 cells, ***p< 0.001, by two-tailed t test). (F) Similar to (E), showing time constants of current inactivation in control or Yoda1 treated mTM cells (n=6-12 cells, **p< 0.01, by two-tailed t test). hTM, human trabecular meshwork cells; mTM, mouse trabecular meshwork cells. The dotted line indicates the zero current level.

resulting changes in gene expression profiles. Piezo1 channel mRNA, but not Piezo2 message, was significantly upregulated after 3 h of stretch (Figure 1F), suggesting a functional role in the TM. Several TRP (transient receptor potential cation) channels, such as TRPA1, TRPC1, TRPC6, TRPV4, and TRPP2, were also upregulated after cyclic stretch, consistent with previous observations of their role in mechanotransduction (Ranade et al., 2015).

Mechanical stimulation activates Piezo1 currents in human and mouse TM cells

To further examine the function of Piezo1 in the TM, we mechanically stimulated human and mouse primary TM cells and performed whole-cell patch-clamp recordings. We first confirmed the TM phenotype in both human and mouse TM cells, verifying robust expression of TM biomarkers and dexamethasone-induced myocilin secretion, assayed by RT-PCR, IHC, and western blotting (Figures S2 and S3), as in our previous publication (Yu et al., 2019). We observed that mechanical stimulation caused currents with fast activation and inactivation kinetics (Figure 2A). Current density in human TM cells increased in response to 6-μm cellular indentation, and a similar (although more rapid) response was observed in mouse TM cells (Figure 2B), following which Yoda1 (10 μM) or GsMTx4 (2.5 μM) were delivered to cells. Treatment of TM cells with Yoda1 (10 μM), a specific agonist for Piezo1 that affects its sensitivity and inactivation kinetics (Syeda et al., 2015), resulted in a significant increase in the mechanosensitive peak current amplitude by about 1.6-fold (-481.7 ± 94.6 versus -297.7 ± 56.1 pA) for human TM cells, and by 2.2-fold (-641.0 ± 200.6 versus -292.7 ± 44.3 pA) for mouse TM cells in response to 6-μm mechanical indentation (Figures 2C and 2D). Furthermore, Yoda1 significantly slowed current inactivation kinetics by about 5-fold (228.1 ± 21.0 versus 46.0 ± 4.5 ms) in human TM cells and by 4-fold (64.5 ± 13.2 versus 16.2 ± 1.9 ms) in mouse TM cells (Figures 2E and 2F). We note that Yoda1 has a half maximal effective concentration [EC_{50}] of 17 and 27 μM for mouse and human Piezo1, respectively (Syeda et al., 2015), similar to the 10 μM used in this study.

We next used the Piezo1 antagonist GsMTx4 (2.5 μM), observing a significant reduction of Piezo1 current amplitude ($57.5\% \pm 7.1\%$ decrease in human primary TM cells and $59.6\% \pm 7.1\%$ decrease in mouse primary TM cells; Figures 2C and 2D) after mechanical indentation. We note that the delivered concentrations of GsMTx4 (2.5 μM) were in the effective range, because GSMTx4 inhibits Piezo1 at micromolar concentrations (Bae et al., 2011). We further down-regulated Piezo1 expression by infecting with an Ad5 virus carrying Piezo1 short hairpin RNA (shRNA) (shRNA-Piezo1) and green fluorescent protein (GFP; Figure S5), and chose the successfully infected HTM cells, i.e., GFP-positive cells, to record mechanically activated (MA) current by whole-cell patch-clamp recordings (Figure S6). As shown in Figure S6, Piezo1 knockdown led to a significant ($66.0\% \pm 7.3\%$) decrease in MA current amplitude due to 6-μm mechanical indentation. As Piezo1 was not completely knocked down by Ad5-shRNA-Piezo1 infection (Figure S5C), we can state that complete Piezo1 knockdown would cause an MA current reduction of more than 66%. These results demonstrate that the Piezo1 channel is functional in both human and mouse primary TM cells.

GsMTx4 leads to a significant decrease in steady-state aqueous outflow facility

To examine the role of mechanosensitive channels (MSCs) in regulating conventional outflow, we delivered GsMTx4, an inhibitor of cationic MSCs, into the anterior chamber of mouse eyes and quantified its effect on aqueous outflow facility. Outflow facility is the numerical inverse of tissue hydrodynamic flow resistance and is the most important measure of TM function. GsMTx4 (3.3 or 10 μM) was perfused unilaterally, whereas the

contralateral eye received control (vehicle) solution. Importantly, our methodology measures quasi-steady outflow facility, i.e., the facility after the eye has equilibrated in response to a pressure perturbation. Although inhibition of MSCs by GsMTx4 (3.3 μM) did not change facility significantly (control: 3.86[2.57, 5.79] versus treated: 4.94[3.33, 7.31] nl/min/mmHg, p = 0.19, n = 10), GsMTx4 at a higher concentration (10 μM) significantly decreased the steady-state facility to 2.78[2.12, 3.64] from 6.37[4.65, 8.73] nl/min/mmHg (n = 10, p = 0.0001; Figure 3). As shown in a "cello plot," the facility in 10 μM GsMTx4-treated eyes changed on average by −56% [-67, −41] relative to control (Figure 3). We note that drugs delivered into the anterior chamber mix with AH already present within the eye, so that the drug concentration delivered to the meshwork is less than the perfused concentration. Our calculations indicate that, over the timescale of a perfusion experiment, the drug concentration delivered to the TM is approximately half of that perfused into the eye (data not shown). Thus we chose to deliver GsMTx4 at concentrations of 3.3 and 10 μM to achieve micromolar concentrations at the target tissue. We conclude that suppression of MSC function by GsMTx4 has a significant effect on AH outflow.

Piezo1 activation did not influence steady-state aqueous outflow facility

Because GsMTx4 is active against several MSCs, the earlier results do not specifically demonstrate a role for Piezo1 in influencing AH dynamics, and we thus wished to more specifically perturb the function of Piezo1 in conventional outflow tissues. To this end, a specific agonist for Piezo1, Yoda1, was perfused into mouse eyes at nominal concentrations of 20 or 40 μM, and the steady-state facility was measured. As before, the contralateral eye was used as a paired control. As Yoda1 is hydrophobic, we were concerned that it might bind to tubing in the iPerfusion system, leading to non-effective delivery of Yoda1 to the eye. Thus, solution delivered through 20 cm of polyethylene (PE) tubing, similar to that used in the iPerfusion system, was collected and analyzed by mass spectrometry. Yoda1 was detected in both samples, indicating that Yoda1 can be delivered to the eye in perfusion experiments (Figure S4). Furthermore, we were concerned that Piezo1 in TM cells may not be abundant. However, Syeda et al. (2015) showed that Piezo1 activity can be monitored using calcium-sensitive fluorophores and that Yoda1 administration alone induces robust Ca^{2+} responses in cells with abundant Piezo1. We thus measured Yoda1-induced intracellular Ca^{2+} level in TM cells, finding that Yoda1 administration alone induced robust Ca^{2+} responses in TM cells (Figure S7), suggesting the presence of abundant Piezo1 in these cells. However, as shown in Figure 4, Yoda1 (20 or 40 μM) did not affect steady-state outflow facility (p = 0.61 for 20 μM Yoda1 and p = 0.82 for 40 μM Yoda1). Moreover, Yoda1 had no significant effect on the flow-pressure nonlinearity parameter β (data not shown). Even after accounting for intracameral drug dilution effects (see above), these observations demonstrate that Piezo1 activation does not play a role in directly influencing steady-state AH outflow.

GsMTx4 affects the eye's response to a pressure perturbation

As Piezo1-induced MA currents are rapid and transient (Figure 2), we next investigated the role of Piezo1 in the eye's rapid response to pressure changes, quantified through ocular compliance, a quantity that is based on transient pressure-flow data after an IOP perturbation (Figure 5A). Interestingly, GsMTx4 (10 μM) increased ocular compliance (53.9 [49.9, 58.2] versus 45.4 [37.8, 54.5] *nl/mmHg*, p = 0.0015, n = 10; Figure 5B). However, 20 μM Yoda1 showed no significant effect on ocular compliance (45.9 [40.0, 52.8] versus 49.1 [43.4, 55.5] *nl/mmHg*, p = 0.22, n = 8; Figure 5C). These observations indicate that MSCs affect the eye's transient pressure-flow response after a pressure perturbation, but that we could not detect a specific role for Piezo1 in this response.

DISCUSSION

The TM and inner wall of SC, centrally involved in determining IOP and hence of great interest in the study of glaucoma, experience large mechanical deformation and are known to be mechanosensitive. Several mechanosensing systems/pathways responders have already been identified in these tissues, including integrin deformation (Filla et al., 2017), nitric oxide signaling (Cavet et al., 2014), caveolin signaling (Elliott et al., 2016), and mechanosensitive ion channels (Tran et al., 2014). Mechanosensitive ion channels are of interest due to their ability to respond very rapidly to mechanical stimuli (Suchyna, 2017), important in view of the dynamic mechanical environment within the eye due to blinks, saccades, and the ocular pulse (Turner et al., 2019).
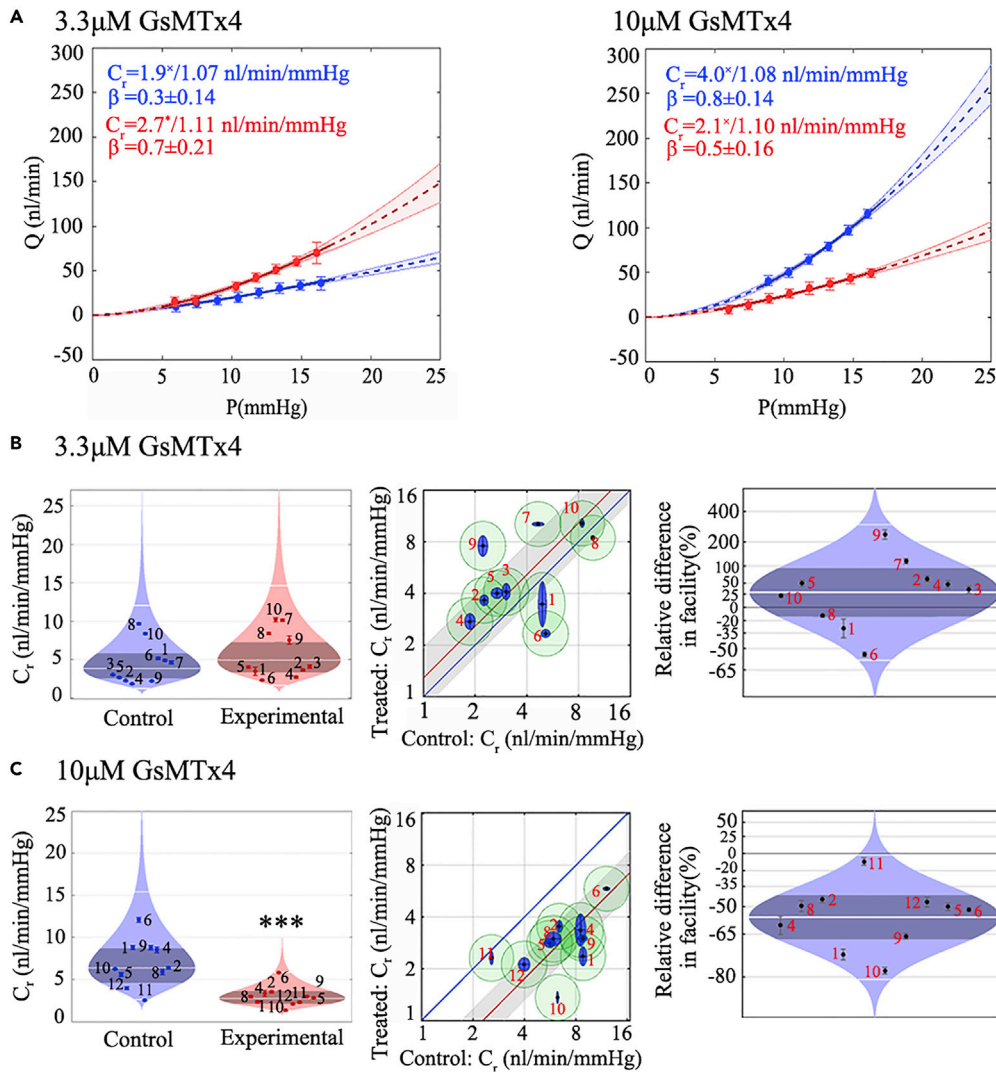
Figure 3. GsMTx4 significantly reduced steady-state outflow facility

(A) Representative flow-pressure curves from two pairs of enucleated mouse eyes receiving GsMTx4 (left: 3.3 μM; right: 10 μM; red) and the correspondingly contralateral vehicle-treated control eyes (blue). Data points are fitted with an existing relationship (see text), with the shaded region showing associated 95% confidence limits (Sherwood et al, 2019).

(B) Left: "Cello plot" of steady-state outflow facility in GsMTx4 (3.3 μM)-injected eyes and their contralateral controls. Each data point shows the reference facility, in one eye, with error bars showing standard deviation. Shaded regions indicate the best estimates of the sample distribution, with the geometric mean and two-sigma shown by the thick and thin horizontal lines, respectively. Dark central bands show the 95% confidence interval on the mean. No significant difference was detected due to 3.3 μM GsMTx4 (control: vs. treated:,). Middle: "Unity plot", showing reference outflow facility in each 3.3 μM GsMTx4-treated eye cross-plotted against facility in the contralateral control eye. Each data point represents one pair of eyes. Filled ellipses indicate 95% confidence intervals from the regression fitting, and outer ellipses indicate additional uncertainty due to hardware noise. The unity line is shown in blue and a linear regression through the data points is shown in red, with its 95% confidence interval in grey. Right: Plot of the relative difference between treated and contralateral control eyes, showing that 3.3 GsMTx4μM led to only a mild (29% [-14, 94]) change in facility that was not statistically different from zero.

(C) Similar to panel (B), showing the effects of 10 μM GsMTx4. Treated eyes exhibited a significantly lower facility than contralateral control eyes (vs., which corresponded to approximately a -56% [-67, -41] reduction. ***$p < 0.001$, by two-tailed t-test on log-transformed data.
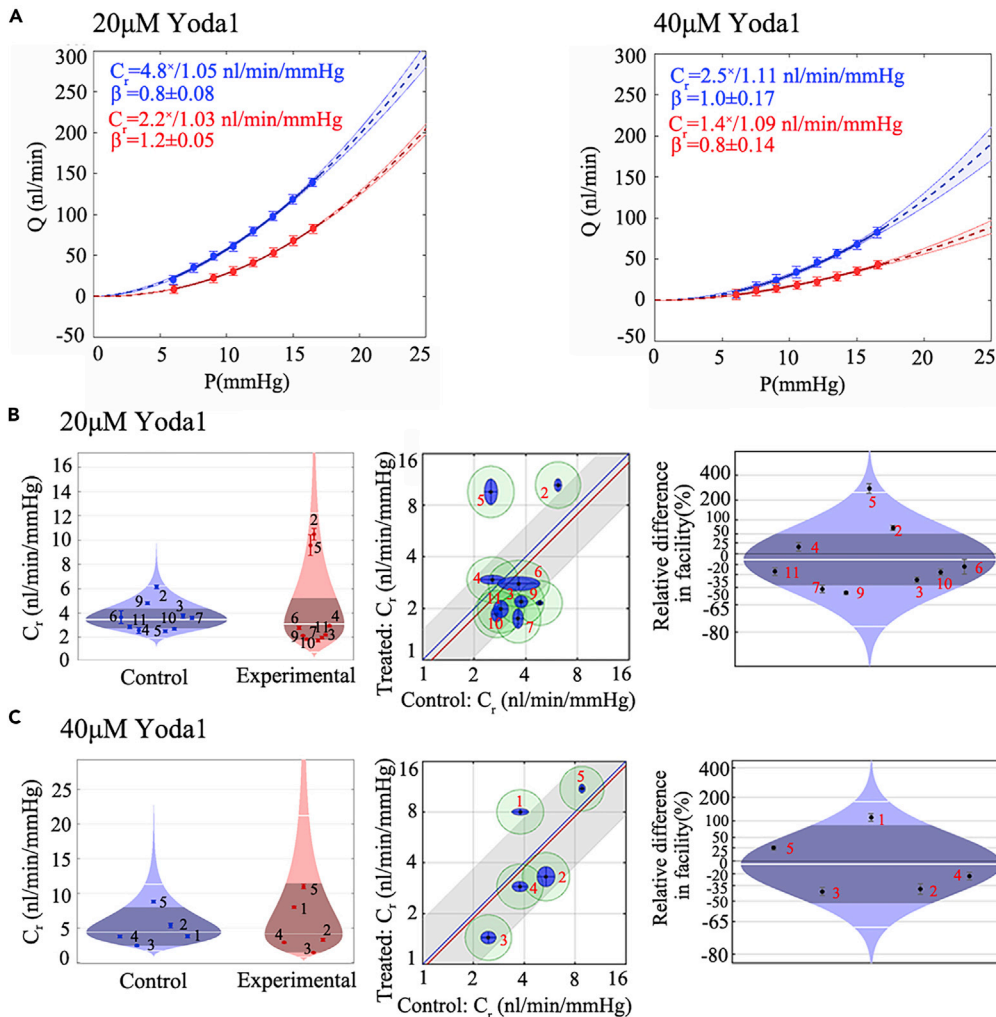
Figure 4. Activation of Piezo1 by Yoda1 did not influence steady-state AH outflow facility

(A) Two sets of representative flow-pressure curves from pairs of enucleated mouse eyes receiving Yoda1 (left: 20 μM; right: 40 μM; red) and their correspondingly contralateral vehicle-treated control eyes (blue). Data points are fitted with an existing relationship (see text), with the shaded region showing associated 95% confidence limits.

(B) Yoda1 (20 μM) treatment did not lead to a significant change in steady-state facility when compared with vehicle control (3.08 [1.81, 5.24] versus 3.46 [2.75, 4.36] $nl/min/mmHg$, p = 0.61, n = 9).

(C) Similar to (B), for 40 μM Yoda1 (4.14 [1.49, 11.47] versus 4.40 [2.43, 7.96] $nl/min/mmHg$, p = 0.82, n = 5). p values were calculated based on a two-tailed t test. Refer to Figure 3 for detailed interpretation of plots.

Recent investigations have demonstrated a functional role for other stretch-activated ion channels in the outflow pathway, including TRPV4's role in regulating calcium homeostasis and TM cytoskeletal remodeling (Carreon et al., 2017; Ryskamp et al., 2016; Tran et al., 2014) and the role of TREK1 in influencing TM tensile homeostasis and extracellular matrix components (Yarishkin et al., 2019). Here we extend these earlier findings to study the fast-acting Piezo1 channel. We observed that Piezo1 was expressed in human and mouse iridocorneal angle tissues, including the TM, SC, ciliary muscle, and ciliary body (Figures 1 and S1), all of which are involved in AH dynamics (Borras, 2003; Civan and Macknight, 2004; Crawford and Kaufman, 1987; Johnson et al., 1992; Stamer et al., 2015). We focused on the TM due to its critical role in mediating AH outflow and maintaining IOP homeostasis (Goel et al., 2010; Tran et al., 2014; WuDunn, 2009). Not only was Piezo1 expressed in TM but also our electrophysiological findings showed that it is a functionally active and rapid mechanosensor in the TM, with MA currents induced within microseconds that were strongly influenced by Piezo1 shRNA (Figures S5 and S6), GsMTx4, and Yoda1 (Figure 2). Furthermore, when challenged by a physiologically appropriate cyclic mechanical stretch, both Piezo1 and TRP family
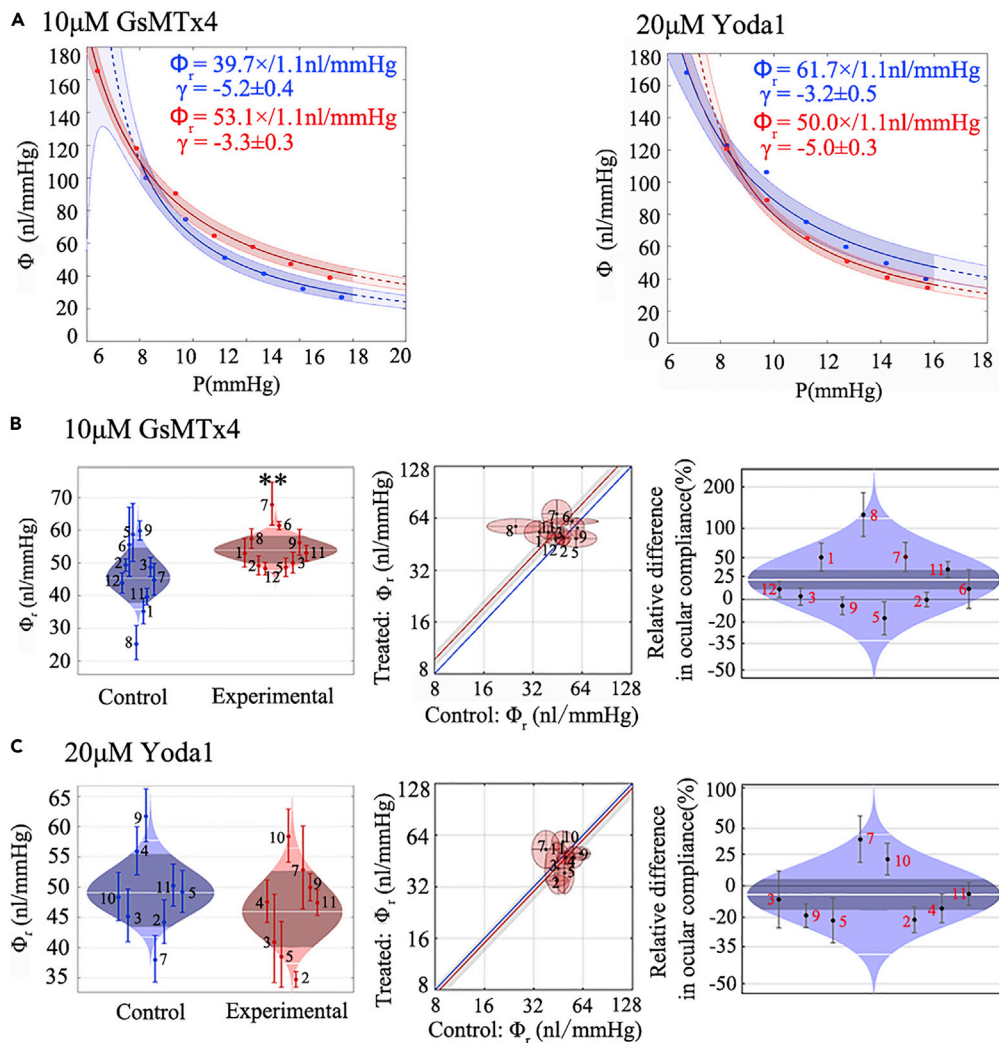
Figure 5. GsMTx4 significantly increases ocular compliance

(A) Two sets of representative compliance-pressure curves generated from eyes receiving either 10 μM GsMTx4 (left, red) or 20 μM Yoda1 (right, red), and the corresponding contralateral vehicle control eyes (blue). Data points are fitted with an existing relationship (see text) and shaded regions show 95% confidence bounds.

(B) 10 μM GsMTx4 led to a significant increase in ocular compliance vs. vehicle control (vs.,).

(C) 20 μM Yoda1 did not change ocular compliance vs vehicle control (vs.,). **p < 0.01. p values were calculated based on a two-tailed t test. Refer to Figure 3 for interpretation of plots.

members were upregulated in TM cells within hours (Figure 1F). These results demonstrate that ion channels, including Piezo1, are functional within TM cells and thus have the potential to be mechanotransducers of AH dynamics.

Surprisingly, we did not, however, find that perturbation of Piezo1 affected steady-state aqueous outflow facility. Specifically, we used the iPerfusion system, which can monitor microvolumetric changes of AH dynamics in the mouse eye (Sherwood et al., 2016), to investigate the effects on conventional outflow of antagonists and agonists against Piezo1 (Figure 3). As described in a newly published study (Yarishkin et al., 2020), we also observed a facility effect of GsMTx4, but unfortunately this inhibitor of cationic ion channels (Bae et al., 2011) can act on many channels, such as TRPs, ASICs, G-protein receptors, and Nox2 (Inoue et al., 2009; Kurima et al., 2015; Suchyna, 2017; Sukharev et al., 1993). For example, TRP channels in muscle were investigated by using GsMTx4 to inhibit whole-cell currents (Friedrich et al., 2012) and GsMTx-4 peptide was used to block the activation of TRPC6 channels (Spassova et al., 2006). Regarding our

electrophysiological findings in TM cells treated with Piezo1 shRNA (Figures S5 and S6), Piezo1 was primarily responsible for inducing MA currents in TM cells, because when Piezo1 was partially knocked down using shRNA, MS currents were reduced by 66%. We infer that GsMTx4, which induced a 57% MA current reduction, acts by interfering with Piezo1 activity. We thus cannot unambiguously determine the role of Piezo1 in AH outflow from these results. Therefore, we next used Yoda1, a specific agonist for Piezo1, yet did not observe any change in steady-state outflow facility due to Yoda1 (Figure 4).

In view of the abundance of Piezo1 in TM, this finding was surprising, and we considered several possible explanations. One possibility is that Yoda1 at nominal concentrations of 20 and 40 μM functions ineffectively in the eye due to absorption of this hydrophobic compound to tubing upstream of the eye, a particularly critical concern in view of the small flow rates and volumes used when perfusing mouse eyes, and the dilution issue in the anterior chamber. However, mass spectrometry showed that Yoda1 did successfully pass through tubing similar to that used in the ocular perfusion experiments (Figure S4). Furthermore, our electrophysiological results (Figure 2) showed that Yoda1, at nominal concentrations of 10 μM, delivered through PVC-based tubing effectively activated Piezo1 in the TM cells. As the PE-based tubing used in our ocular perfusion system has relatively low adsorption to hydrophobic drugs (Jin et al., 2017; Syeda et al., 2015), we conclude that the absence of effects seen with Yoda1 were likely not due to delivery issues into the eye. Furthermore, we observed Yoda1-increased MA currents (Figure 2) and Yoda1-induced intracellular calcium levels (Figure S7), confirming that Yoda1 (carrier-free, Sigma-Aldrich, SML 1558) is able to cause a downstream reaction.

A second possibility relates to the timescale of our measurements. We hypothesized that Piezo1 is specifically responsible for rapid adjustments in aqueous outflow, consistent with its rapid response in cultured TM cells (Figure 2). Recalling that facility data described above were obtained under quasi-steady conditions, we therefore analyzed transient pressure-flow data in mouse eyes, as quantified through ocular compliance. Usually ocular compliance is thought to depend exclusively on the biomechanical properties of the corneoscleral shell, but can also be affected by transient changes in aqueous outflow during the measurement period (Sherwood et al., 2019). We found that GsMTx4 significantly increased ocular compliance (Figure 5), but Yoda1 did not. Previous investigations have suggested that Piezo1 can significantly regulate extracellular matrix and reinforce tissue stiffening (Chen et al., 2018), which could affect ocular compliance through an effect on the sclera. However, this seems implausible on the timescale of our experiments, and thus changes in outflow dynamics mediated by MSCs are a more likely explanation for the effect of GsMTx4 on ocular compliance. Despite these findings, our observation of dynamic changes in outflow appears not to be mediated by Piezo1, because Yoda1 did not affect ocular compliance. However, this may be due to a limitation of our measurement capabilities: the transient analysis of flow-pressure data that we report requires data collection over a timescale of several minutes, which is much longer than the timescale for Piezo1-derived MA currents (<1 s, Figure 2). A more complete elucidation of Piezo1's role in the TM will require development of functional assays with response times of order a second or less, comparable with the timescale of blinks, saccades, and the ocular pulse.

A final possible explanation for our findings is that activation of Piezo1 in the TM of normal mice, as used in our study, is essentially maximal during facility measurement. In this situation, Yoda1 would not be able to further increase Piezo1 activity and thus would not influence facility. It is possible that the effects of Yoda1 would only become evident under pathological conditions, such as occur in ocular hypertension, and conducting such studies would be of great interest.

In summary, our results confirm the role of mechanosensitive ion channels in regulation of conventional steady-state AH outflow. Piezo1, as one such channel, is widely expressed and is functional in TM, yet its specific activation appears to have little effect on quasi-steady outflow facility. These results suggest that Piezo1 may be important in mechanoregulation of AH dynamics in pathological situations and in response to very rapid ocular changes, such as commonly occur due to ocular saccades and other events.

Limitations of the study

Our study demonstrates the potential role for Piezo1 in conventional outflow, likely under pathological and rapid transient conditions. However, the transient analysis of flow-pressure data that we report requires data collection over a timescale of several minutes, which is much longer than the timescale for Piezo1-derived MA currents (<1 s). A more complete elucidation of Piezo1's role in the TM will require development of functional assays with response times of order a second or less, comparable with the timescale of blinks, saccades, and the ocular pulse.

Resource availability

Lead contact

Further requests for resources and materials should be direct to the Lead Contact, Wei Zhu (wzhu@qdu.edu.cn).

Materials availability

Requests for materials should be direct to the Lead Contact.

Data and code availability

The raw data are available on Mendeley Data (https://doi.org/10.17632/5v2mbp2sdx.1).

METHODS

All methods can be found in the accompanying Transparent methods supplemental file.

SUPPLEMENTAL INFORMATION

Supplemental Information can be found online at https://doi.org/10.1016/j.isci.2021.102042.

AUTHOR CONTRIBUTIONS

W. Zhu (first author) and F.H. conceived and designed the project. W. Zhu, J.F., M.R.B.F., and J.M.S. conducted the facility measurement and statistical analysis. Y.L. and S.S. performed the patch-clamp recording. F.H., S.W., and S.R. conducted RT-PCR and western blot. A.T.R., W. Zou, H.Y., and J.Z. conducted IHC experiment. Y.Q. carried out the mass spectrometry analysis. C.R.E., D.R.O., N.W., and K.W. contributed to result analysis and discussions. The manuscript was written by W. Zhu, C.R.E., and K.W.

DECLARATION OF INTERESTS

All authors do not have any conflicts of interest to declare.

REFERENCES

Bae, C., Sachs, F., and Gottlieb, P.A. (2011). The mechanosensitive ion channel Piezo1 is inhibited by the peptide GsMTx4. Biochemistry 50, 6295–6300.

Borras, T. (2003). Gene expression in the trabecular meshwork and the influence of intraocular pressure. Prog. Retin. Eye Res. 22, 435–463.

Buckingham, B.P., Inman, D.M., Lambert, W., Oglesby, E., Calkins, D.J., Steele, M.R., Vetter, M.L., Marsh-Armstrong, N., and Horner, P.J. (2008). Progressive ganglion cell degeneration precedes neuronal loss in a mouse model of glaucoma. J. Neurosci. 28, 2735–2744.

Cahalan, S.M., Lukacs, V., Ranade, S.S., Chien, S., Bandell, M., and Patapoutian, A. (2015). Piezo1 links mechanical forces to red blood cell volume. Elife 4, e07370.

Carreon, T.A., Castellanos, A., Gasull, X., and Bhattacharya, S.K. (2017). Interaction of cochlin and mechanosensitive channel TREK-1 in trabecular meshwork cells influences the regulation of intraocular pressure. Sci. Rep. 7, 452.

Cavet, M.E., Vittitow, J.L., Impagnatiello, F., Ongini, E., and Bastia, E. (2014). Nitric oxide (NO): an emerging target for the treatment of glaucoma. Invest. Ophthalmol. Vis. Sci. 55, 5005–5015.

Chandler, P.A. (1977). Progress in the treatment of glaucoma in my lifetime. Surv. Ophthalmol. 21, 412–428.

Chen, X., Wanggou, S., Bodalia, A., Zhu, M., Dong, W., Fan, J.J., Yin, W.C., Min, H.K., Hu, M., Draghici, D., et al. (2018). A feedforward mechanism mediated by mechanosensitive ion Channel PIEZO1 and tissue mechanics promotes glioma aggression. Neuron 100, 799–815.e7.

Civan, M.M., and Macknight, A.D.C. (2004). The ins and outs of aqueous humour secretion. Exp. Eye Res. 78, 625–631.

Coste, B., Houge, G., Murray, M.F., Stitziel, N., Bandell, M., Giovanni, M.A., Philippakis, A., Hoischen, A., Riemer, G., Steen, U., et al. (2013). Gain-of-function mutations in the mechanically activated ion channel PIEZO2 cause a subtype of Distal Arthrogryposis. Proc. Natl. Acad. Sci. U S A 110, 4667–4672.

Coste, B., Mathur, J., Schmidt, M., Earley, T.J., Ranade, S., Petrus, M.J., Dubin, A.E., and Patapoutian, A. (2010). Piezo1 and Piezo2 are essential components of distinct mechanically activated cation channels. Science 330, 55–60.

Crawford, K., and Kaufman, P.L. (1987). Pilocarpine antagonizes prostaglandin F2 alpha-induced ocular hypotension in monkeys. Evidence for enhancement of Uveoscleral outflow by prostaglandin F2 alpha. Arch. Ophthalmol. 105, 1112–1116.

Eijkelkamp, N., Linley, J.E., Torres, J.M., Bee, L., Dickenson, A.H., Gringhuis, M., Minett, M.S., Hong, G.S., Lee, E., Oh, U., et al. (2013). A role for Piezo2 in EPAC1-dependent mechanical allodynia. Nat. Commun. 4, 1682.

Eisenhoffer, G.T., Loftus, P.D., Yoshigi, M., Otsuna, H., Chien, C.B., Morcos, P.A., and Rosenblatt, J. (2012). Crowding induces live cell extrusion to maintain homeostatic cell numbers in epithelia. Nature 484, 546–549.

Elliott, M.H., Ashpole, N.E., Gu, X., Herrnberger, L., McClellan, M.E., Griffith, G.L., Reagan, A.M., Boyce, T.M., Tanito, M., Tamm, E.R., and Stamer, W.D. (2016). Caveolin-1 modulates intraocular pressure: implications for caveolae mechanoprotection in glaucoma. Sci. Rep. 6, 37127.

Filla, M.S., Faralli, J.A., Peotter, J.L., and Peters, D.M. (2017). The role of integrins in glaucoma. Exp. Eye Res. 158, 124–136.

Friedrich, O., Wagner, S., Battle, A.R., Schürmann, S., and Martinac, B. (2012). Mechano-regulation of the beating heart at the cellular level—mechanosensitive channels in normal and diseased heart. Prog. Biophys. Mol. Biol. 110, 226–238.

Goel, M., Picciani, R.G., Lee, R.K., and Bhattacharya, S.K. (2010). Aqueous humor dynamics: a review. Open Ophthalmol. J. 4, 52–59.

Hirt, J., and Liton, P.B. (2017). Autophagy and mechanotransduction in outflow pathway cells. Exp. Eye Res. 158, 146–153.

Ikeda, R., Cha, M., Ling, J., Jia, Z., Coyle, D., and Gu, J.G. (2014). Merkel cells transduce and encode tactile stimuli to drive Abeta-afferent impulses. Cell 157, 664–675.

Inoue, R., Jian, Z., and Kawarabayashi, Y. (2009). Mechanosensitive TRP channels in cardiovascular pathophysiology. Pharmacol. Ther. 123, 371–385.

Jin, S.E., You, S., Jeon, S., Byon, H.J., and Hwang, S.J. (2017). Evaluation of drug sorption to PVC- and non-PVC-based tubes in administration sets using a pump. J. Vis. Exp. 55086.

Johnson, M., Shapiro, A., Ethier, C.R., and Kamm, R.D. (1992). Modulation of outflow resistance by the pores of the inner wall endothelium. Invest. Ophthalmol. Vis. Sci. 33, 1670–1675.

Johnstone, M.A. (2004). The aqueous outflow system as a mechanical pump: evidence from examination of tissue and aqueous movement in human and non-human primates. J. Glaucoma 13, 421–438.

Kerr, J., Nelson, P., and O'Brien, C. (2003). Pulsatile ocular blood flow in primary open-angle glaucoma and ocular hypertension. Am. J. Ophthalmol. 136, 1106–1113.

Koser, D.E., Thompson, A.J., Foster, S.K., Dwivedy, A., Pillai, E.K., Sheridan, G.K., Svoboda, H., Viana, M., Costa, L.D., Guck, J., et al. (2016). Mechanosensing is critical for axon growth in the developing brain. Nat. Neurosci. 19, 1592–1598.

Kurima, K., Ebrahim, S., Pan, B., Sedlacek, M., Sengupta, P., Millis, B.A., Cui, R., Nakanishi, H., Fujikawa, T., Kawashima, Y., et al. (2015). TMC1 and TMC2 localize at the site of mechanotransduction in mammalian inner ear hair cell stereocilia. Cell Rep. 12, 1606–1617.

Lee, W., Leddy, H.A., Chen, Y., Lee, S.H., Zelenski, N.A., McNulty, A.L., Wu, J., Beicker, K.N., Coles, J., Zauscher, S., et al. (2014). Synergy between Piezo1 and Piezo2 channels confers high-strain mechanosensitivity to articular cartilage. Proc. Natl. Acad. Sci. U S A 111, E5114–E5122.

Li, J., Hou, B., Tumova, S., Muraki, K., Bruns, A., Ludlow, M.J., Sedo, A., Hyman, A.J., McKeown, L., Young, R.S., et al. (2014). Piezo1 integration of vascular architecture with physiological force. Nature 515, 279–282.

Liton, P.B., and Gonzalez, P. (2008). Stress response of the trabecular meshwork. J. Glaucoma 17, 378–385.

Lukacs, V., Mathur, J., Mao, R., Bayrak-Toydemir, P., Procter, M., Cahalan, S.M., and Kim, H.J. (2015). Impaired PIEZO1 Function in patients with a novel autosomal recessive congenital lymphatic dysplasia. Nat. Commun. 6, 8329.

Martins, J.R., Penton, D., Peyronnet, R., Arhatte, M., Moro, C., Picard, N., Kurt, B., Patel, A., Honore, E., and Demolombe, S. (2016). Piezo1-dependent regulation of urinary osmolarity. Pflugers Arch. 468, 1197–1206.

Nonomura, K., Woo, S.H., Chang, R.B., Gillich, A., Qiu, Z., Francisco, A.G., Ranade, S.S., Liberles, S.D., and Patapoutian, A. (2017). Piezo2 senses airway stretch and mediates lung inflation-induced apnoea. Nature 541, 176–181.

Pathak, M.M., Nourse, J.L., Tran, T., Hwe, J., Arulmoli, J., Le, D.T., Bernardis, E., Flanagan, L.A., and Tombola, F. (2014). Stretch-activated ion channel Piezo1 directs lineage choice in human neural stem cells. Proc. Natl. Acad. Sci. U S A 111, 16148–16153.

Ramos, R.F., Sumida, G.M., and Stamer, W.D. (2009). Cyclic mechanical stress and trabecular meshwork cell contractility. Invest. Ophthalmol. Vis. Sci. 50, 3826–3832.

Ranade, S.S., Qiu, Z., Woo, S.H., Hur, S.S., Murthy, S.E., Cahalan, S.M., Xu, J., Mathur, J., Bandell, M., Coste, B., et al. (2014a). Piezo1, a mechanically activated ion channel, is required for vascular development in mice. Proc. Natl. Acad. Sci. U S A 111, 10347–10352.

Ranade, S.S., Syeda, R., and Patapoutian, A. (2015). Mechanically activated ion channels. Neuron 87 (6), 1162–1179.

Ranade, S.S., Woo, S.H., Dubin, A.E., Moshourab, R.A., Wetzel, C., Petrus, M., Mathur, J., Begay, V., Coste, B., Mainquist, J., et al. (2014b). Piezo2 is

the major transducer of mechanical forces for touch sensation in mice. Nature 516, 121–125.

Retailleau, K., Duprat, F., Arhatte, M., Ranade, S.S., Peyronnet, R., Martins, J.R., Jodar, M., Moro, C., Offermanns, S., Feng, Y., et al. (2015). Piezo1 in smooth muscle cells is involved in hypertension-dependent arterial remodeling. Cell Rep. 13, 1161–1171.

Ryskamp, D.A., Frye, A.M., Phuong, T.T., Yarishkin, O., Jo, A.O., Xu, Y., Lakk, M., Iuso, A., Redmon, S.N., Ambati, B., et al. (2016). TRPV4 regulates calcium homeostasis, cytoskeletal remodeling, conventional outflow and intraocular pressure in the mammalian eye. Sci. Rep. 6, 30583.

Sherwood, J.M., Boazak, E.M., Feola, A.J., Parker, K., Ethier, C.R., and Overby, D.R. (2019). Measurement of ocular compliance using iPerfusion. Front. Bioeng. Biotechnol. 7, 276.

Sherwood, J.M., Reina-Torres, E., Bertrand, J.A., Rowe, B., and Overby, D.R. (2016). Measurement of outflow facility using iPerfusion. PLoS One 11, e0150694.

Sihota, R., Angmo, D., Ramaswamy, D., and Dada, T. (2018). Simplifying "target" intraocular pressure for different stages of primary open-angle glaucoma and primary angle-closure glaucoma. Indian J. Ophthalmol. 66, 495–505.

Smith, R.S., Zabaleta, A., Savinova, O.V., and John, S.W. (2001). The mouse anterior chamber angle and trabecular meshwork develop without cell death. BMC Dev. Biol. 1, 3.

Spassova, M.A., Hewavitharana, T., Xu, W., Soboloff, J., and Gill, D.L. (2006). A common mechanism underlies stretch activation and receptor activation of TRPC6 channels. Proc. Natl. Acad. Sci. U S A 103, 16586–16591.

Stamer, W.D., Braakman, S.T., Zhou, E.H., Ethier, C.R., Fredberg, J.J., Overby, D.R., and Johnson, M. (2015). Biomechanics of Schlemm's canal endothelium and intraocular pressure reduction. Prog. Retin. Eye Res. 44, 86–98.

Suchyna, T.M. (2017). Piezo channels and GsMTx4: two milestones in our understanding of excitatory mechanosensitive channels and their role in pathology. Prog. Biophys. Mol. Biol. 130, 244–253.

Sukharev, S.I., Martinac, B., Arshavsky, V.Y., and Kung, C. (1993). Two types of mechanosensitive channels in the Escherichia coli cell envelope: solubilization and functional reconstitution. Biophys. J. 65, 177–183.

Syeda, R., Xu, J., Dubin, A.E., Coste, B., Mathur, J., Huynh, T., Matzen, J., Lao, J., Tully, D.C., Engels, I.H., et al. (2015). Chemical activation of the mechanotransduction channel Piezo1. Elife 4, e07369.

Tran, V.T., Ho, P.T., Cabrera, L., Torres, J.E., and Bhattacharya, S.K. (2014). Mechanotransduction channels of the trabecular meshwork. Curr. Eye Res. 39, 291–303.

Turner, D.C., Edmiston, A.M., Zohner, Y.E., Byrne, K.J., Seigfried, W.P., Girkin, C.A., Morris, J.S., and Downs, J.C. (2019). Transient intraocular pressure fluctuations: source, magnitude, frequency, and

associated mechanical energy. Invest. Ophthalmol. Vis. Sci. *60*, 2572–2582.

Weinreb, R.N., Aung, T., and Medeiros, F.A. (2014). The pathophysiology and treatment of glaucoma: a review. JAMA *311*, 1901–1911.

Woo, S.H., Lukacs, V., de Nooij, J.C., Zaytseva, D., Criddle, C.R., Francisco, A., Jessell, T.M., and Wilkinson, K.A. (2015). Piezo2 is the principal mechanotransduction channel for proprioception. Nat. Neurosci. *18*, 1756–1762.

Woo, S.H., Ranade, S., Weyer, A.D., Dubin, A.E., Baba, Y., Qiu, Z., Petrus, M., Miyamoto, T., Reddy, K., Lumpkin, E.A., et al. (2014). Piezo2 is required for Merkel-cell mechanotransduction. Nature *509*, 622–626.

WuDunn, D. (2009). Mechanobiology of trabecular meshwork cells. Exp. Eye Res. *88*, 718–723.

Yarishkin, O., Baumann, J.M., and Krizaj, D. (2019). Mechano-electrical transduction in trabecular meshwork involves parallel activation of TRPV4 and TREK-1 channels. Channels (Austin) *13*, 168–171.

Yarishkin, O., Phuong, T.T.T., Baumann, J.M., De Ieso, M.L., Vazquez-Chona, F., Rudzitis, C.N., Sundberg, C., Lakk, M., Stamer, W.D., and Krizaj, D. (2020). Piezo1 channels mediate trabecular meshwork mechanotransduction and promote aqueous fluid outflow. J. Physiol. https://doi.org/10.1113/jp281011.

Yarishkin, O., Phuong, T.T.T., Bretz, C.A., Olsen, K.W., Baumann, J.M., Lakk, M., Crandall, A., Heurteaux, C., Hartnett, M.E., and Krizaj, D. (2018). TREK-1 channels regulate pressure sensitivity and calcium signaling in trabecular meshwork cells. J. Gen. Physiol. *150*, 1660–1675.

Yu, H., Miao, Y., Chen, W., Qi, X., Yang, X., Pan, X., Wang, K., and Zhu, W. (2019). Expressional and functional involvement of gap junctions in aqueous humor outflow into the ocular trabecular meshwork of the anterior chamber. Mol. Vis. *25*, 255–265.
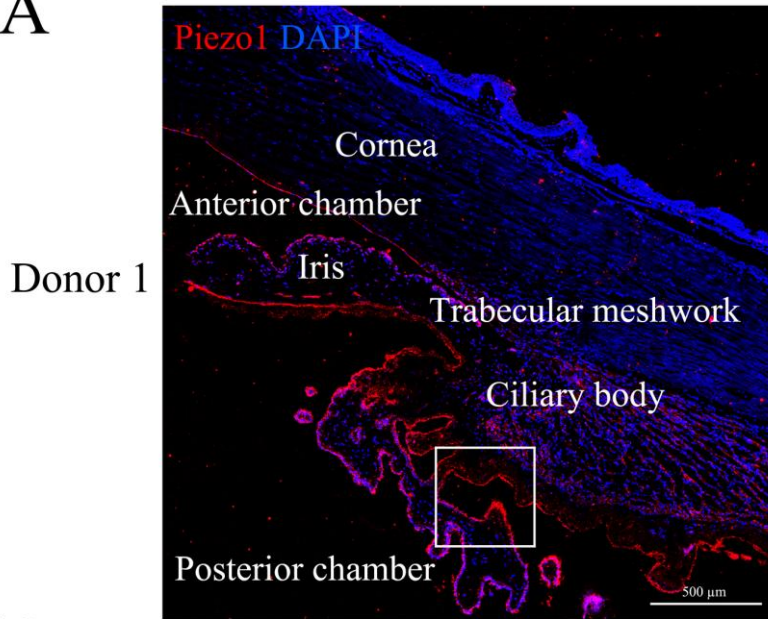
Supplemental Information

The role of Piezo1
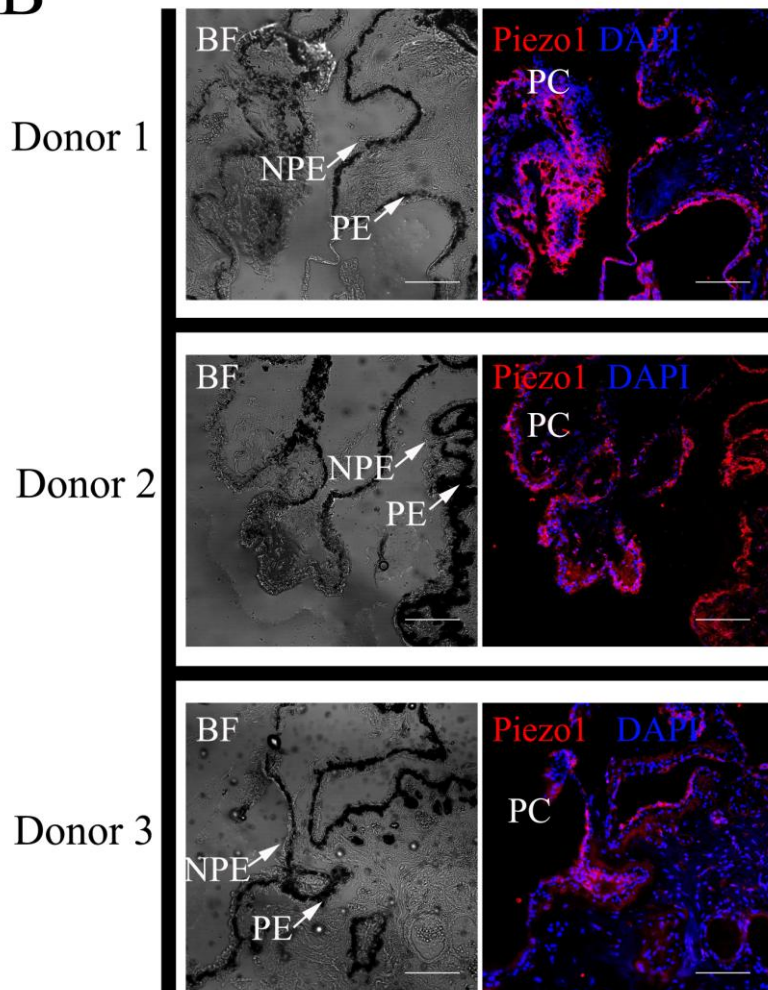
in conventional aqueous

humor outflow dynamics

Wei Zhu, Fei Hou, Jingwang Fang, Mohammad Reza Bahrani Fard, Yani Liu, Shouyan Ren, Shen Wu, Yunkun Qi, Shangru Sui, A. Thomas Read, Joseph M. Sherwood, Wei Zou, Hongxia Yu, Jingxue Zhang, Darryl R. Overby, Ningli Wang, C. Ross Ethier, and KeWei Wang

1   **Figure S1**

A

Donor 1

Piezo1 DAPI

Cornea

Anterior chamber

Iris

Trabecular meshwork

Ciliary body

Posterior chamber

500 μm

B

Donor 1

BF

NPE

PE

Piezo1 DAPI

PC

Donor 2

BF

NPE

PE

Piezo1 DAPI

PC

Donor 3

BF

NPE

PE

Piezo1 DAPI

PC

2

Figure S1. Piezo1 is expressed in the human ciliary body, related to Figure 1. A. Confocal immunofluorescent microscopy of the anterior segment of a human eye showing Piezo1 immunofluorescence (red) and DAPI nuclei (blue). The ciliary body region is identified by a white frame, corresponding to higher magnification images in panel B. Scale bar: 500 μm. **B.** Positive staining of Piezo1 was observed in epithelial cells of the ciliary body (n=3), especially in non-pigmented epithelium cells. Scale bars: 100 μm. BF: Bright field. PC: posterior chamber. PE: pigmented epithelium. NPE: non-pigmented epithelium.

11 **Figure S2**
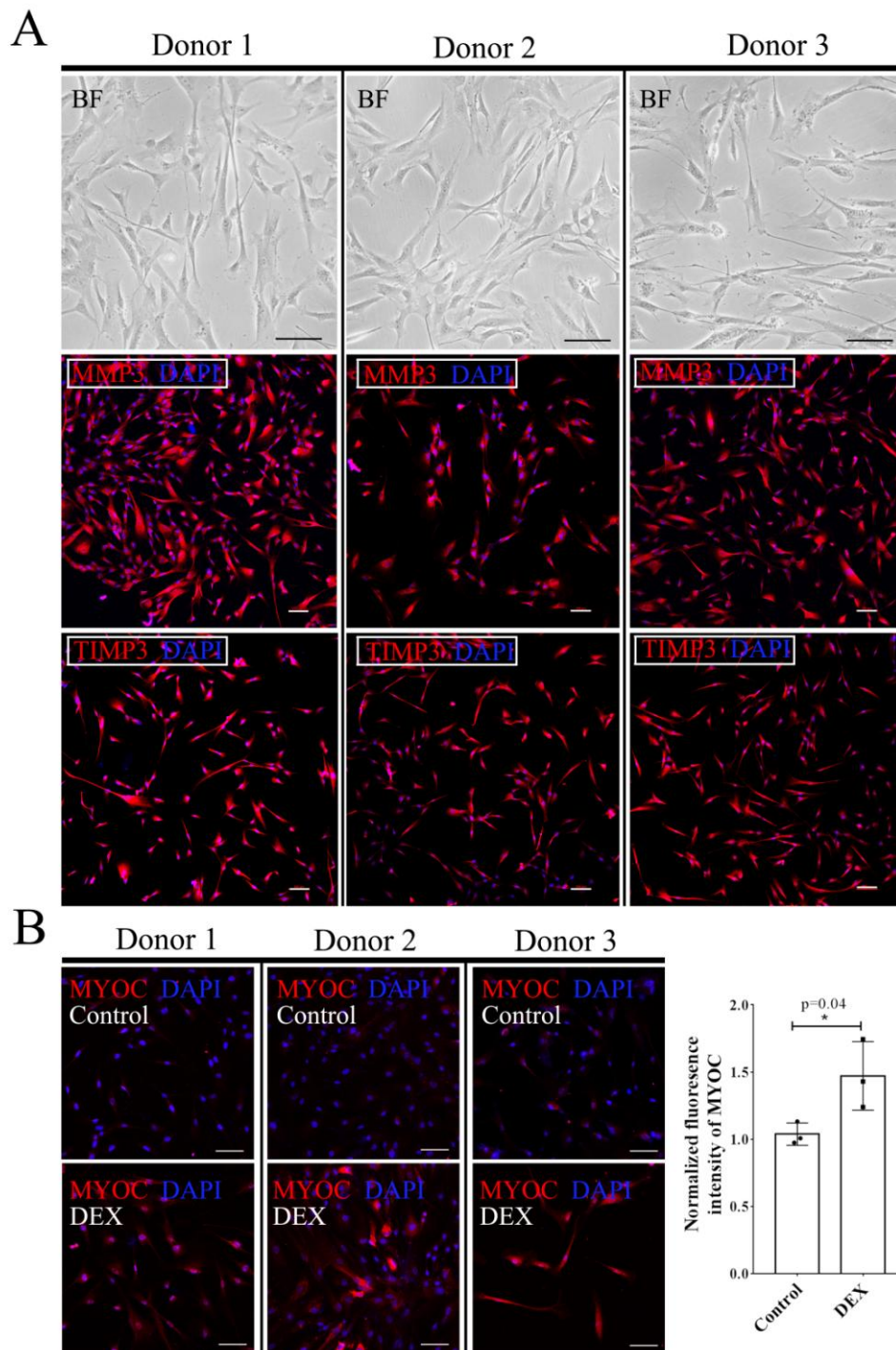
12

13 **Figure S2. Characterization of human TM (HTM) cells, related to Figure 1 and 2.**
14 **A.** Representative morphological and immunohistochemical images of human TM
15 cells from donors 4-6 showing spindle-like cell morphology and immunofluorescence
16 due to labeling of TM biomarkers (MMP3 and TIMP3, red). Scale bars: 100 μm. BF
17 = bright field. **B.** Myocilin (MYOC) expression levels in dexamethasone (DEX)-
18 treated HTM cells and vehicle controls were quantified through IHC analysis.
19 Experiments were repeated three times using HTM cells (n=3). *$P<0.05$, by two-
20 tailed t-test.
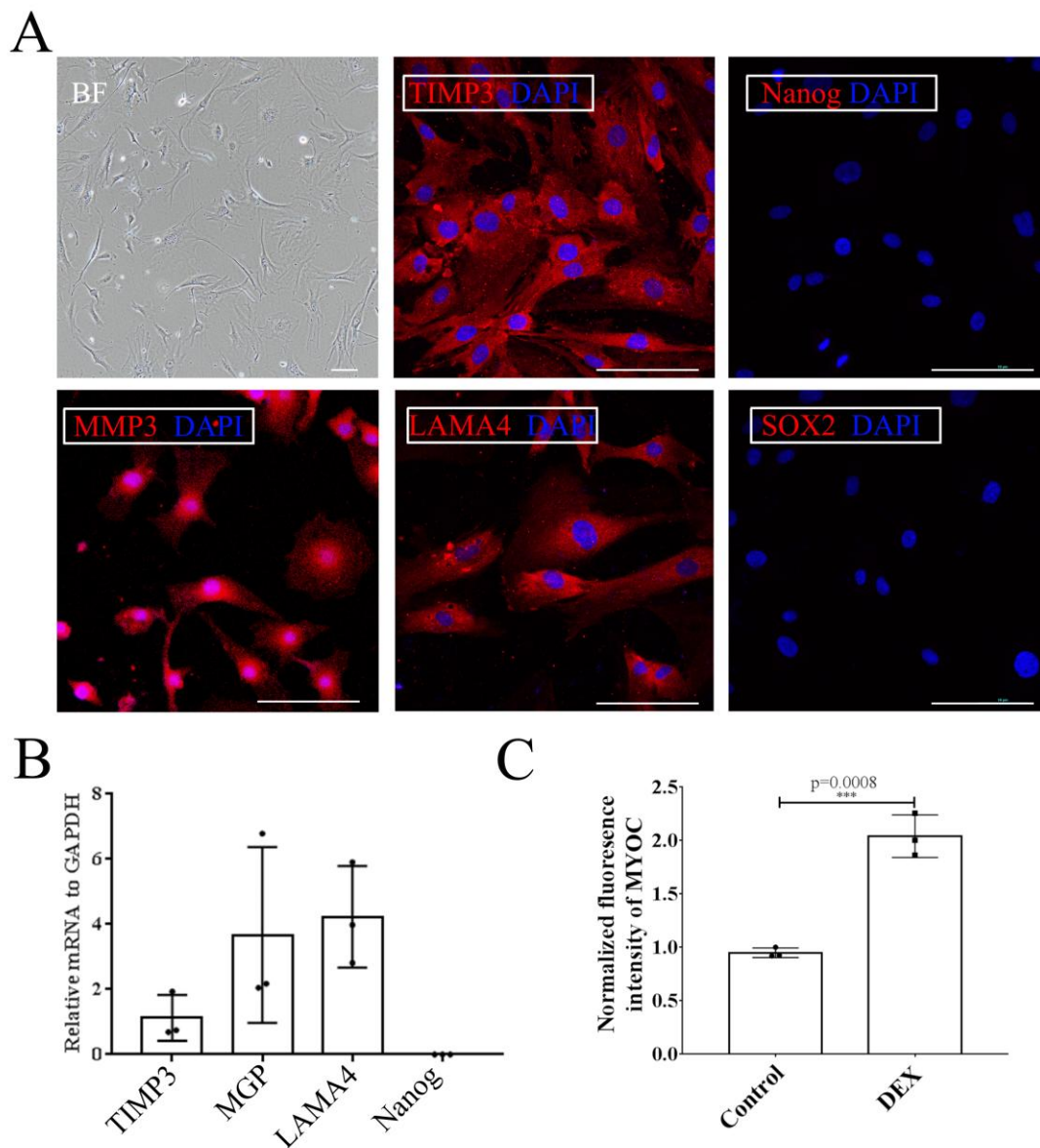
21   **Figure S3**

Figure S3. Characterization of mouse TM cells, related to Figure 1 and 2. A. Representative IHC images of mouse TM cells showing immunofluorescence due to labeling of TM biomarkers (LAMA4 and TIMP3, red). Nuclei were labeled with DAPI (blue). No expression of stem cell biomarkers, Nanog and Sox2, was detected in these cells. Scale bars: 100 μm. BF = bright field. **B.** Transcript levels for the TM biomarkers, TIMP3, MGP, LAMA4, and a stem cell biomarker, Nanog, were quantified in mouse TM cells by RT-PCR. Experiments were repeated three times by using pooled TM cells from 20 mouse eyes. **C.** Myocilin (MYOC) expression in dexamethasone (DEX)-treated cells, and in vehicle-treated control cells was quantified through IHC analysis. Experiments were repeated three times by using mouse TM cells (n=3). *P<0.05, by two-tailed t-test.

34 **Figure S4**
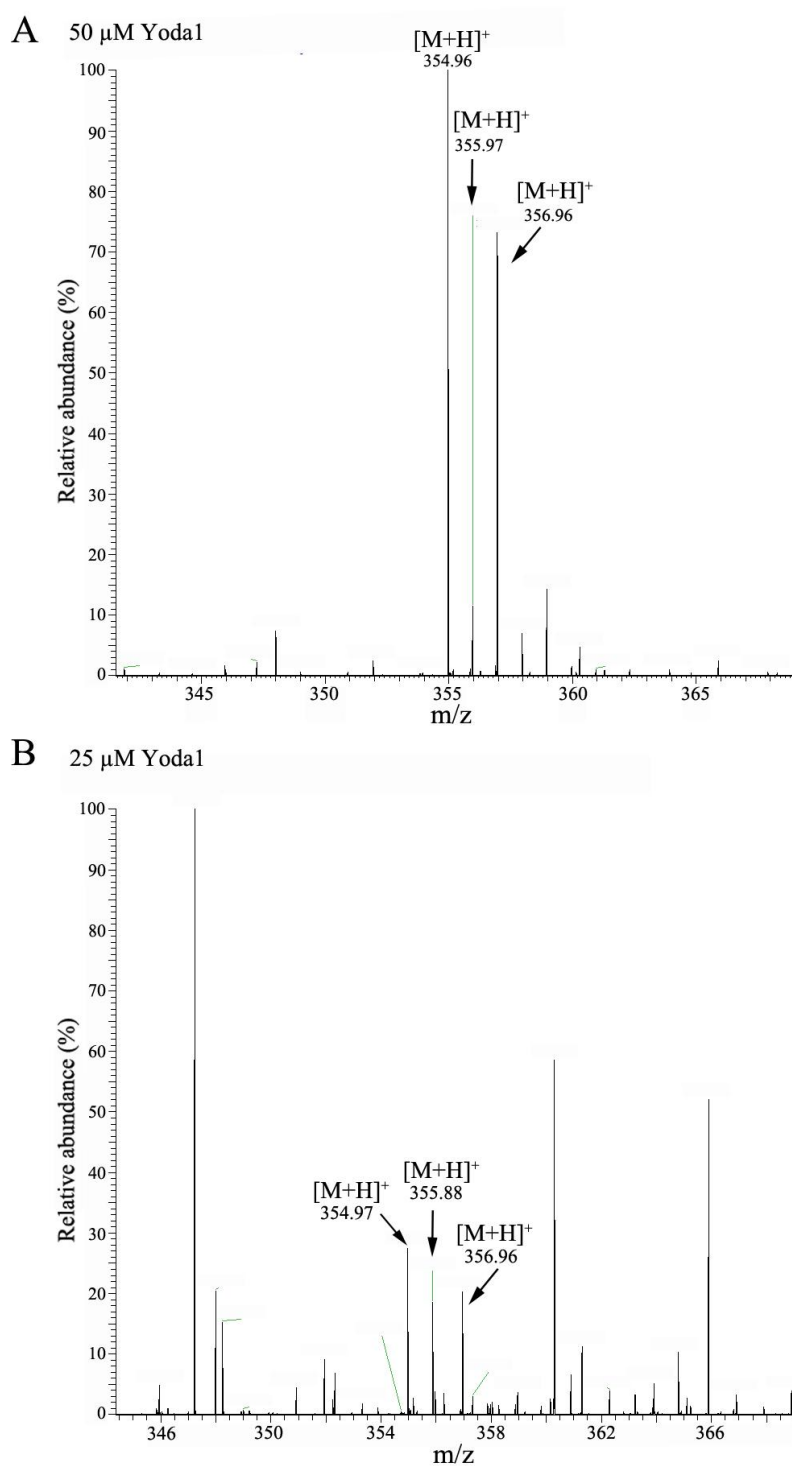
35

36 **Figure S4. Verification of Yoda1 in perfusate after passage through tubing,**
37 **related to Figure 4 and 5.** Mass spectrometry was used to verify that Yoda1 (A: 50
38 μM; B: 25 μM) was being delivered through tubing similar to that used during ocular
39 perfusion studies. Yoda1-containing solution was flowed through the same type and
40 length of tubing as used in the iPerfusion system and the effluent was analyzed. The
41 [M+H]$^+$ data of Yoda1 observed from 354.96 to 355.96 Daltons were detected.

42   **Figure S5**
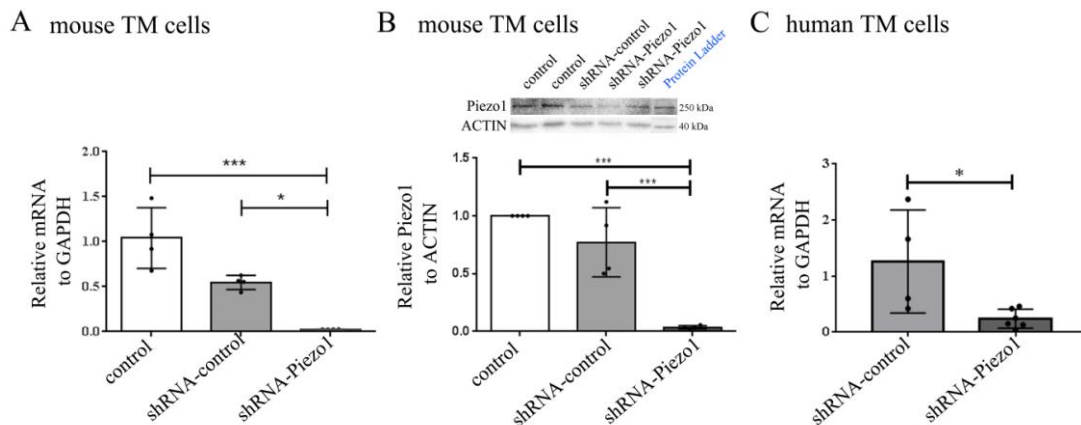
43

44   **Figure S5. Expression of Piezo1 in mouse TM cells transfected with Piezo1**
45   **shRNA, related to Figure 2. A.** Significantly decreased Piezo1 transcript levels in
46   mouse TM cells infected with Ad5 virus carrying Piezo1 shRNA (shRNA-Piezo1)
47   compared to cells treated with Ad5 carrying scrambled shRNA (shRNA-control) as
48   determined by RT-PCR analysis (n=4). *$p<0.05$, ***$p< 0.001$. *p* values were
49   determined from one-way ANOVA. **B.** Top panel: A representative image of a
50   Western blot. Lower panel: Quantification of Western blots, showing significantly
51   decreased Piezo1 protein levels in mouse TM cells treated with Piezo1 shRNA
52   compared to control or scrambled shRNA-control (n=4). *$p<0.05$, ***$p< 0.001$. *p*
53   values were from one-way ANOVA analysis. **C.** Significantly decreased Piezo1
54   transcript levels were observed in human TM cells treated with shRNA, as determined
55   by RT-PCR analysis (shRNA-control: n=4; shRNA-Piezo1: n=6). *$p<0.05$ by two-
56   tailed t-test.

57   **Figure S6**
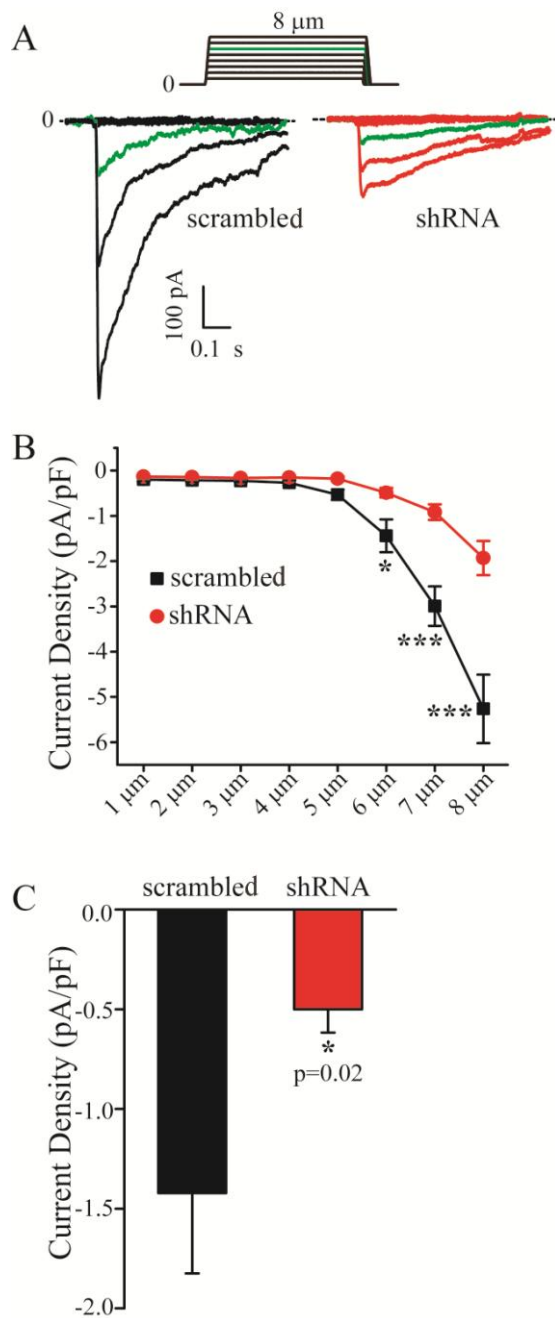
58

59   **Figure S6. Mechanical activation of Piezo1 current in HTM with Piezo1**
60   **knockdown, related to Figure 2. A.** HTM cells treated with either scrambled shRNA
61   (control) or Piezo1 shRNA were subjected to a series of mechanical stimuli consisting
62   of sequential 1 μm indentations. Typical mechanosensitive inward current traces
63   recorded by whole-cell patch-clamp system are shown (n=10 cells). Mechanically
64   activated current at 6 μm indentation is highlighted in green. **B.** Current densities in
65   HTM cells treated with scrambled shRNA (control; black) or Piezo1 shRNA (red) is
66   shown for 8 steps of mechanical stimulation (n=10, *$p < 0.05$, ***$p < 0.001$, by two-
67   tailed t-test). **C.** Piezo1 down-regulation by shRNA led to a significant $66.0 \pm 7.3\%$
68   decrease of MA current amplitude when cells were subjected to 6 μm mechanical
69   indentation (n=10 cells, *$p < 0.05$, by two-tailed t-test).

70   **Figure S7**

HTM of donor4

HTM of donor5

HTM of donor6
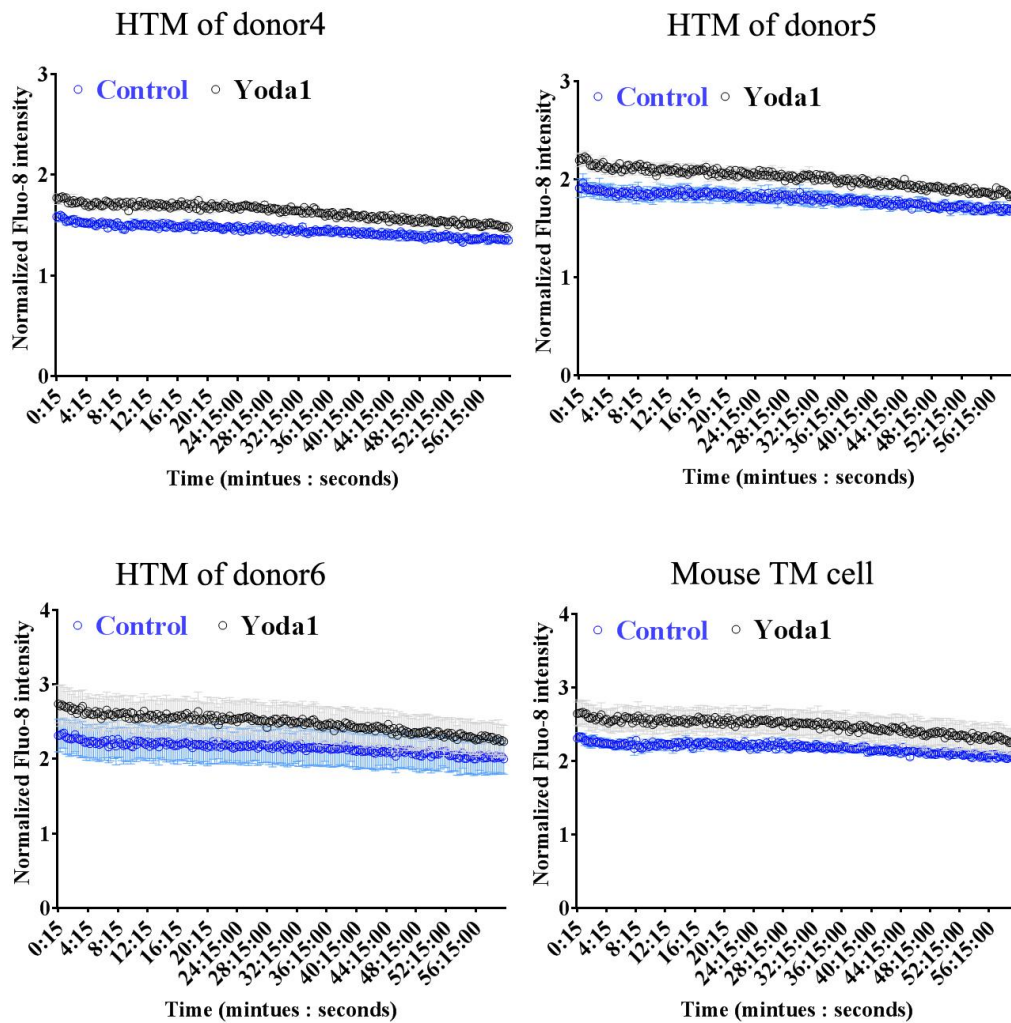
Mouse TM cell

71

72   **Figure S7. Yoda1-induced [Ca^{2+}] upregulation in TM cells, related to Figure 2.**
73   Mouse TM and HTM cells were treated with Yoda1 (20 μM), and labelled with Fluo-
74   8 (5 μM, ab142773) to quantify calcium levels (Flexstation 3 Multi-Mode Microplate
75   Reader). Normalized Fluo-8 intensities (mean and SD) over 1 hour showed that
76   Yoda1 increased intracellular calcium levels in TM cells compared to the vehicle
77   control, suggesting Piezo1 abundance in TM cells(Syeda et al, 2015).

78 **Table S1.** Human donor demographic characteristics. N/A = not available, related to
79 Figure 1.

Donor number	Age	Gender	Race	Cause of Death	Systemic disease	Lions Eye Bank No.	Use in this study
Donor 1	53	Female	Caucasian	Breast cancer	N/A	15-009	Tissue immunohistochemistry
Donor 2	66	Female	Caucasian	Aortic aneurysm	N/A	16-076	Tissue immunohistochemistry
Donor 3	74	Female	Caucasian	Pulmonary edema	Acute respiratory failure with hypoxia, chronic back pain, supraventricular tachycardia, hypersensitivity lung disease, gastroesophageal reflux disease, depression, hypertension, abdominal aortic aneurysm repair	17-009	Tissue immunohistochemistry
Donor 4	80	Male	Caucasian	Acute respiratory distress	N/A	17-056	HTM cell isolation and culture
Donor 5	37	Female	Caucasian	Acute liver failure	N/A	17-062	HTM cell isolation and culture
Donor 6	62	Female	Caucasian	Breast cancer	N/A	14-010	HTM cell isolation and culture

80

81 **Table S2.** Primers for amplification of mechanosensitive ion channels, related to
82 Figure 1.

Gene	Forward	Reverse
hPiezo1	GACCCTCTCGCGACACATAG	CCGAGTGCTGATGGGAAAGT
hPiezo2	CATCTACAGACTGGCCCACC	AGACACTTGAAGCCAGACGG
hTRPA1	GTATTGCAAAGAAGCGGGGC	GCAATTGCTCCACATTGCCA
hTRPC1	TGGTTTGGACAGATGTCGGG	CCTTCTGCCACCAGTGTAGG
hTRPC3	CAGCCAACACGTTATCAGCA	TCCTCAGTTGCTTGGCTCTT
hTRPC6	CGAGAGCCAGGACTATCTGC	CAGCTGCATCCAAAAAGCGT
hTRPV4	GTGGGGAGGCTTTTCCTCTC	GGTGACGATAGGTGCCGTAG
hTRPP2	GATGAAAGGCTGGGTCGTGA	GGGGCGAGGTTGACCATTTA
hTASK1	CATCACCGTCATCACCACCA	CAGCAGGTACCTCACCAAGG
hTREK1	CACGAAACCCACAGTGCTTG	ATGAGGCTGCTCCAATGCTT
hGAPDH	GTCAAGGCTGAGAACGGGAA	AAATGAGCCCCAGCCTTCTC
mPiezo1	TCTGCTGCCTGAGGTATGTG	GGCACCTTTTGCTTCTTCAG
mGAPDH	AACTTTGGCATTGTGGAAGG	ACACATTGGGGGTAGGAACA

83

84   **Table S3.** Information on antibodies used in the study. IHC = immunohistochemistry,
85   WB = Western blot, related to Figure 1.

Name	Brand	Catalog No.	Reactivity	Applications
Anti-Piezo1 antibody	Novus Biologicals	NBP1-78537	Human, Mouse	IHC, WB
Anti-Piezo1 antibody	Proteintech Group Inc	15939-1-AP	Human	WB
Anti-Collagen IV antibody	Abcam	ab6311	Human	IHC
Anti-CD31 antibody	Abcam	ab9498	Human	IHC
Anti-TIMP3 antibody	Abcam	ab39184	Human, Mouse	IHC
Anti-MMP3 antibody	Abcam	ab209675	Human, Mouse	IHC
Anti-LAMA4 antibody	Abcam	ab53015	Human, Mouse	IHC
Anti-MYOC antibody	Abcam	ab41552	Human, Mouse	IHC
Anti-β-actin antibody	Abcam	ab8226	Human, Mouse	WB
Anti-GAPDH antibody	Abcam	ab181602	Human, Mouse	WB

86

87   **Transparent Methods**

88   *Animals*

89   2-month-old male C57BL/6J mice were purchased from the Jackson Laboratory (Bar
90   Harbor, Maine) and Beijing Vital River Laboratory Animal Technology Co, Ltd
91   (Beijing, China), and used for functional tests and mouse TM cell isolation. Mice
92   were housed at either Qingdao University Medical Center (Qingdao, China) or
93   Georgia Institute of Technology under standard conditions with a 12 h/12 h light/dark
94   cycle, at 23 ± 2 ℃ ambient temperature and $55 \pm 10\%$ relative humidity. All
95   experimental procedures conformed to institutional guidelines for laboratory animal
96   care and use, were approved by Qingdao University Medical Center and Georgia
97   Institute of Technology Institutional Animal Care and Use Committee, and conformed
98   to the ARVO Statement for the Use of Animals in Ophthalmic and Vision Research.

99   *Human tissue*

100   Eyes from human donors without known ophthalmic disease (donor numbers 1 to 6),
101   were obtained from the Lions Eye Bank (Iowa City, IA) and used for
102   immunohistochemistry and human TM (HTM) cell isolation. Demographic
103   information about the donors and how tissue was used in this study is shown in Table
104   S1. The protocol for human tissues collection was approved by the Eye Bank
105   Association of America in accordance with the tenets of the Declaration of Helsinki.

106   *Reagents*

107   A specific agonist for Piezo1, Yoda1 (Sigma-Aldrich, St. Louis, MO), and an
108   antagonist GsMTx4 (Abcam, Cambridge, MA) were perfused into mouse anterior
109   chambers to activate or inhibit Piezo1 activity, respectively. The stock solution of
110   Yoda1 (42 mM) was made in DMSO and stored at 4 ℃. Working solutions of Yoda1
111   (20 or 40 μM) were prepared by diluting the stock solution into DBG ($1 \times$ Dulbecco's
112   Phosphate-Buffered Saline [DPBS, Thermo] plus 5.5 mM glucose) which was stored
113   at 37 ℃ for 1 hour before use to ensure complete dissolution of the agonist. The stock
114   solution of GsMTx4 (244 μM) was made in $1 \times$ DPBS and stored at -20 ℃. Fresh
115   working solutions of GsMTx4 (3.3 and 10 μM) were made by diluting the stock
116   solution into DBG.

117   *Mass spectrometry*

118   Yoda1 (25 and 50 μM) solutions were made by diluting the stock solution into
119   ultrapure water. After perfusing solutions through tubing, electrospray ionization (ESI)
120   mass spectrometry was performed in the Mass Spectrometry Center of the Ocean
121   University of China following the manufacturer's suggested protocol (Thermo
122   Scientific Liquid Chromatography Mass Spectrometry; LC-MS; LTQ Orbitrap XL).

123   *Preparation of cryosections*

124   Human eyes were enucleated within 6 hours of death, and experimental procedures
125   were completed within 1 hour after collection. The anterior segments were dissected
126   carefully in a biosafety hood and fixed immediately by immersion in 4%
127   paraformaldehyde (Thermo, Waltham, MA). After rinsing with DPBS (Thermo) and
128   infiltrating with sucrose solutions at a series of concentration of 13.3 %, 15.0 %, and
129   16.7 % (wt/vol), the tissues were embedded in Optimal Cutting Temperature

compound (OCT; Sakura, Tokyo, Japan). The embedded tissues were cryosectioned on a Leica CM1950 at 10 μm thickness (Leica, Nussloch, Germany) for immunohistochemical analysis.

Human primary TM cell isolation

As previously described(Ding et al, 2014), anterior segments were carefully separated from ocular globes in a biosafety hood. The TM tissue, visualized as a brown ring in the iridocorneal angle, was collected with a 0.5 mm curette. After rinsing with Dulbecco's modified eagle medium (DMEM; Gibco, Grand Island, New York), the harvested tissue was digested in DMEM containing 4 mg/ml collagenase A (Sigma-Aldrich) and 4 mg/ml human serum albumin (Sigma-Aldrich) at 37 ℃ for 2 hours. After centrifugation, the pellets were resuspended in human complete medium comprising 199E medium (Gibco), 20% fetal bovine serum (FBS; Gibco), 90 μg/ml porcine heparin (Sigma), 20 U/ml endothelial cell growth supplement (Sigma) and 1.7 mM L-glutamine (Sigma). The digested tissue components were seeded onto 1% gelatin pre-coated 6-well plates (Thermo) and cultured in an incubator with a 5% CO_2 atmosphere at 37 ℃. Cells at passages 5 to 8, characterized according to the described features of TM cells(Yu et al, 2019), were used in this study.

Mouse primary TM cell isolation

Mouse primary TM cells were isolated by a magnetic bead-based approach(Mao et al, 2013) that exploits the avid phagocytic activity of TM cells. Magnetic microspheres (2.0 μm diameter, 50 mg/2 ml; Tianjin Baseline Chromtech Research Center, China) were sterilized in 75% alcohol and suspended in 1×DPBS (Gibco). 2 μl of a 1% (wt/vol) solution of sterile magnetic beads were injected into the mouse anterior chamber(Keller et al, 2018). Mice receiving magnetic beads were sacrificed at the second day after injection, and eyes were dissected carefully under an ophthalmic surgical microscope. The iris and ciliary body were removed from the anterior segment, and the corneoscleral angle tissues were collected. Tissues from approximately 20 eyes were pooled into 1×DPBS (Gibco) containing 4 mg/mL collagenase A (Sigma-Aldrich) and 4 mg/mL human serum albumin (Sigma-Aldrich). After incubation at 37 ℃ for 2 hours, cells with magnetic microspheres were selected by passage through the magnetic LS column sorting system (MACS, Teterow, Germany). The selected cells were cultured in human complete medium in an incubator with 5% CO_2 at 37 ℃. Mouse primary TM cells at passages 3 to 6 were characterized by immunohistochemistry and used in this study.

Mechanical stretch

Human primary TM cells were seeded onto Collagen I-coated Bioflex culture plates (Flexcell International Corporation, Burlington, NC). When cells reached approximately 80% confluence, low serum medium (α-MEM with 1% FBS) was applied for 24 hours before mechanical stimulation. Stretching was delivered with a Flexcell FX-5000TM Tension System (Flexcell International Corporation, Burlington, NC) in a humidified incubator with 5% CO_2 at 37 ℃. Cells were subjected to cyclic mechanical stretch with an amplitude of 20% at 1 Hz (sinusoidal stretch profile). Cells maintained on Bioflex plates under static conditions were used as non-stretched controls.

Real-time PCR (RT-PCR)

Total RNA was extracted using TRIzol reagent (Ambion, Waltham, MA) and quantified with a Nanophotometer (Implen, Germany). cDNAs were generated from mRNA through random primed reverse transcription reaction (Promega, Madison, Wisconsin). The samples were amplified in triplicate using the SYBR Green system (Bio-Rad, Hercules, CA). The primers for amplification of mouse and human *Piezos* were designed using Beacon designer V7.9 and shown in Table S2. *GAPDH* (Gene ID: 2597 OMIM: 138400) was used as a reference gene. The PCR reaction was run at 95 ℃ for 15 min, followed by 50 cycles at 95 ℃ for 10 s, at 50 ℃ for 30 s and at 72 ℃ for 30 s(Coste et al, 2010).

Immunohistochemical staining

Sections from human donors 1 to 3 were rinsed in Dulbecco's PBS (1×; 145 mM NaCl, 8.1 mM $Na_2HPO_4 \cdot 12H_2O$, 1.9 mM $NaH_2PO_4 \cdot 2H_2O$, PH7.2-7.4; DPBS; Thermo) for 5 mins, and incubated in the blocking solution (DPBS with 1% bovine serum albumin, BSA; Sigma) for 1 hour. The sections were further incubated with the diluted primary antibodies (1:100) and the corresponding secondary antibodies (1:200). Cell nuclei were stained with 4′,6-diamidino-2-phenylindole (DAPI; Santa Cruz, Dallas, TX), and the stained sections were mounted using Neutral Balsam (Solarbio, Beijing, China) and imaged by confocal microscopy (Nikon, Tokyo, Japan). The imaged TM tissues were sub-divided into three regions: uveal meshwork, corneoscleral meshwork, and the JCT, based on previous publications.

The primary antibodies used in this study were rabbit polyclonal anti-Piezo1 (Novus, NBP1-78537, Littleton, CO), mouse polyclonal Collagen IV (Abcam, ab6311), and mouse monoclonal anti-CD31 (Abcam, ab9498). The secondary antibodies were rabbit immunoglobulin G (IgG) Alexa Fluor® 568 (Invitrogen, Carlsbad, CA) and mouse IgG Alexa Fluor® 488 (Invitrogen). Information regarding antibodies and their use in this study is summarized in Table S3.

Quantification of Piezo1-positive cells in the TM used high-magnification images (400x) in which the uveal, corneoscleral and juxtacanalicular regions were identified by an expert observer (WZ). Cells labeled positive for Piezo1 in the perinuclear area were automatically detected (StrataQuest software, TissueGnostics GmbH, Austria) and counted. The number of positive cells in each region was divided by the total number of cells in that region, as determined by DAPI staining.

Western blotting

Proteins were extracted from TM tissues or primary TM cells using RIPA buffer supplemented with Halt™ Protease Inhibitor Cocktail (Thermo). Total protein was quantified using the BSA Protein Reagent Kit (Thermo). 20μg total protein was loaded on a 5% sodium dodecyl sulfate (SDS)-acrylamide stacking gel. Proteins were separated on a 10% SDS-acrylamide gel by electrophoresis and transferred to a polyvinyl difluoride membrane (PVDF; GE Healthcare, Boston, MA) using a Trans-blot Turbo Transfer system (Bio-Rad) at 200 mA current for 90 min. PVDF membranes were incubated with blocking buffer at room temperature for 1 hour before further incubation with primary antibodies against Piezo1 (Proteintech, Rosemont, IL) at 4 ℃ overnight. After rinsing with Tris-buffered Saline-Tween-20 (TBST) three times, the membrane was incubated with the corresponding secondary antibody conjugated with horseradish peroxidase (HRP; Abcam) at room temperature

220   for 1 hour. Immunoreactive bands were visualized using SuperSignal West Pico
221   PLUS Chemiluminescent Substrate (Thermo). Band intensity was quantified by the
222   Imagelab imaging system (Bio-Rad) and normalized to the amount of GAPDH or β-
223   actin.

Electrophysiology

225   Whole-cell patch-clamp recordings from human and mouse primary TM cells were
226   performed at room temperature. Patch electrodes were pulled using a horizontal
227   micropipette puller (P-97, Sutter Instruments, Novato, CA) and fire-polished to a
228   resistance of 2-5 MΩ. Mechanical stimulation was delivered using a blunt fire-
229   polished glass pipette with 3-4 μm outer diameter that was positioned at an angle of
230   80 ° respect to horizontal. Downward movement of the pipette was controlled by a
231   Clampexcontrolled piezo-electric crystal microstage (E625 LVPZT
232   Controller/Amplifier; Physik Instrumente, Germany). A series of mechanical
233   indentations with increasing amplitudes (1 μm increments) was applied. The velocity
234   of the pipette was 0.5 μm/ms, and the stimulus was maintained for 600 ms, after
235   which the pipette was withdrawn for 9.4 s before applying the next stimulus, i.e. a
236   stimulus was applied every 10 seconds. The intracellular recording solution included
237   140 mM KCl, 5 mM EGTA, 2 mM $MgCl_2$, 10 mM HEPES, 2 mM Mg-ATP, pH 7.3.
238   The extracellular recording bath solution included 140 mM NaCl, 4 mM KCl, 2 mM
239    $CaCl_2$, 1 mM $MgCl_2$, 10 mM Glucose, 10 mM HEPES, pH 7.4. Mechanical currents
240   were recorded using a MultiClamp 700B amplifier and pCLAMP 10.0 software
241   (Molecular Devices, San Jose, CA) at a holding potential of -80 mV. Yoda1 (10 μM)
242   or GsMTx4 (2.5 μM) were delivered to the chamber containing the cells through a
243   gravity perfusion system (ALA Scientific Instruments, Farmingdale, NY) consisting
244   of polyvinyl choloride (PVC) tubing with a length of 30 cm.

Detection of intracellular calcium

246   Cells were seeded in 96-well plates (mouse TM: 9400 cells/well, HTM from donor 4:
247   5600 cells/well, HTM from donor 5: 4800 cells/well, HTM from donor 6: 6400
248   cells/well), cultured in human complete medium for 2 days and starved in MEM-α for
249   2 hours before incubation with Fluo-8 (5 μM, Abcam, ab142773) at 37 ℃ for 1 hour.
250   Yoda1 (20 μM) or DMSO vehicle control (0.1 %) were then added and fluorescence
251   intensities were immediately recorded for 1 hour at 15-second intervals by a
252   Flexstation 3 Multi-Mode Microplate Reader (Molecular Devices, LLC. San Jose,
253   CA). Experiments were technically repeated four times in each cell line using mouse
254   TM cells and HTM cells (n=3). Fluo-8 intensity reads in each group were normalized
255   by dividing by Fluo-8 intensity in a blank group. Normalized reads over the 1 hour
256   interval were averaged for the statistical analysis.

Preparation of Adenovirus 5 (Ad5)

258   To create the recombinant adenovirus 5 construct, oligonucleotides (targeting
259   sequence: CACCGGCATCTACGTCAAATA for silencing of mouse Piezo1,
260   scrambled sequence: TTCTCCGAACGTGTCACGT) were cloned into the pDC311-
261   U6-MCMV-EGFP vector (Shanghai Hanbio Technology Co., Ltd, China). The
262   pDC311 vector with either shRNA mPiezo1 or scrambled shRNA and pBHGlox E1,3
263   constructs (Hanbio, China) were co-transfected into HEK293 cells using LipoFiter^{TM}
264   transfection reagents (Hanbio, China) to generate the recombinant virus. The
265   propagated recombinant adenoviruses were purified from HEK293 cells and the virus

266 titer was measured by standard plaque assays. We prepared stock solutions of Ad5
267 containing 1×10^{11} plaque formation unit (PFU)/ml.

Infection of Ad5 carrying siRNA mPiezo1

269 5,000 mouse TM cells at passage 3 were cultured in 12-well plates, infected by
270 recombinant adenoviruses carrying mouse Piezo1 shRNA at 300 multiplicity of
271 infection (MOI) for 6 hours, recovered in human complete medium for 120 hours, and
272 collected for real-time PCR and Western blot analysis.

Outflow facility measurement

274 Mouse eyes were enucleated and mounted on eye holders in an iPerfusion system(Zhu
275 et al, 2017), which comprises an actuated pressure reservoir, a pressure transducer
276 (PX409, Omegadyne, USA) and a thermal flow meter (SLG0150, Sensirion,
277 Switzerland). A glass microneedle with 40-80 μm inner diameter was prepared by a
278 horizontal micropipette puller (P-97, Sutter Instruments, Novato, CA) and BV-10
279 microelectrode beveler (World Precision Instruments, Hertfordshire, England).
280 Anterior chambers of eyes were cannulated and eyes were perfused with a DBG
281 solution at 8 mmHg for 45 minutes ($1 \times$ DPBS plus 5.5 mM glucose; Sigma), followed
282 by nine sequential pressure steps of 4.5, 6, 7.5, 9, 10.5, 12, 13.5, 15, 16.5 mmHg. At
283 each step, flow rate (Q) and pressure (P) in the eye were recorded until the slope in
284 the plot of flow rate vs. time was less than 3 nl/min/min for 60 seconds. Finally, a
285 pressure of 8 mmHg was applied to the eye to monitor the eye's return to baseline.

286 Following previous methodology(Zhu et al, 2017), a power-law model was fit to the
287 measured flow-pressure data to account for the pressure-dependency of outflow
288 facility

$$Q\,(P) = C_r \left(\frac{P}{P_r}\right)^{\beta} P$$

289 In the above equation, P_r is a reference pressure (taken as 8 mmHg) with
290 corresponding outflow facility C_r, and β is a parameter that characterizes the non-
291 linearity of the flow-pressure relationship. The flow rate and pressure during the last 4
292 minutes of each step were used for power law fitting, and thus the facility values that
293 we report should be considered quasi-steady facilities.

Ocular compliance

295 In addition to the quasi-steady facility of the eye, measured as described above, we
296 considered the transient response of the eye to changes in IOP. One approach to such
297 an analysis is to consider the ocular compliance (ϕ), which describes the pressure-
298 volume relationship of the eye following a perturbation in ocular pressure or volume.
299 The transient pressure-flow data from facility experiments was analyzed according to
300 existing techniques(Sherwood et al, 2019). As is the case for facility, ocular
301 compliance depends on ocular pressure, and hence at each pressure step, a value of ϕ
302 was determined using the discrete volume approach(Sherwood et al, 2019). The
303 compliance-pressure data were then fit by the equation:

$$\phi(P) = \phi_r \left\{\frac{P_{r,\phi} + \gamma}{P + \gamma}\right\}$$

304 where $P_{r,\phi}$ is a reference pressure (taken as 13 mmHg) at which the ocular compliance
305 is ϕ_r. γ is an empirical fitting parameter(Sherwood et al, 2019).

Statistical analysis

307 The Shapiro-Wilk test was used to test for normality. A two-tailed *t*-test was applied
308 for statistical analysis of electrophysiological data. One-way ANOVA was performed
309 for statistical analysis of Piezo1-positive cell ratio data and the expression levels of
310 mechanosensitive ion channels after cyclic mechanical stretch. A two-tailed *t*-test was
311 used for statistical analysis of normalized Fluo-8 intensity data. All tests were
312 performed in GraphPad Prism 8. A two-tailed *t*-test was also used to analyze the log-
313 transformed outflow facility and ocular compliance data, which was accomplished in
314 MATLAB. p values < 0.05 were considered to be statistically significant.
315 Electrophysiological data were expressed as the mean ± SEM, and Fluo-8 intensity
316 data were presented as the mean ± SD. Oular perfusion data were expressed as the
317 mean [lower bound of 95% CI, upper bound of 95% CI].

318

References

Coste, B., Mathur, J., Schmidt, M., Earley, T. J., Ranade, S., Petrus, M. J., Dubin, A. E. & Patapoutian, A. (2010) Piezo1 and Piezo2 are essential components of distinct mechanically activated cation channels. *Science*, 330(6000), 55-60.

Ding, Q. J., Zhu, W., Cook, A. C., Anfinson, K. R., Tucker, B. A. & Kuehn, M. H. (2014) Induction of trabecular meshwork cells from induced pluripotent stem cells. *Invest Ophthalmol Vis Sci*, 55(11), 7065-72.

Keller, K. E., Bhattacharya, S. K., Borras, T., Brunner, T. M., Chansangpetch, S., Clark, A. F., Dismuke, W. M., Du, Y., Elliott, M. H., Ethier, C. R., Faralli, J. A., Freddo, T. F., Fuchshofer, R., Giovingo, M., Gong, H., Gonzalez, P., Huang, A., Johnstone, M. A., Kaufman, P. L., Kelley, M. J., Knepper, P. A., Kopczynski, C. C., Kuchtey, J. G., Kuchtey, R. W., Kuehn, M. H., Lieberman, R. L., Lin, S. C., Liton, P., Liu, Y., Lutjen-Drecoll, E., Mao, W., Masis-Solano, M., McDonnell, F., McDowell, C. M., Overby, D. R., Pattabiraman, P. P., Raghunathan, V. K., Rao, P. V., Rhee, D. J., Chowdhury, U. R., Russell, P., Samples, J. R., Schwartz, D., Stubbs, E. B., Tamm, E. R., Tan, J. C., Toris, C. B., Torrejon, K. Y., Vranka, J. A., Wirtz, M. K., Yorio, T., Zhang, J., Zode, G. S., Fautsch, M. P., Peters, D. M., Acott, T. S. & Stamer, W. D. (2018) Consensus recommendations for trabecular meshwork cell isolation, characterization and culture. *Exp Eye Res*, 171, 164-173.

Mao, W., Liu, Y., Wordinger, R. J. & Clark, A. F. (2013) A magnetic bead-based method for mouse trabecular meshwork cell isolation. *Invest Ophthalmol Vis Sci*, 54(5), 3600-6.

Sherwood, J. M., Boazak, E. M., Feola, A. J., Parker, K., Ethier, C. R. & Overby, D. R. (2019) Measurement of Ocular Compliance Using iPerfusion. *Frontiers in Bioengineering and Biotechnology*, 7(276).

Syeda, R., Xu, J., Dubin, A. E., Coste, B., Mathur, J., Huynh, T., Matzen, J., Lao, J., Tully, D. C., Engels, I. H., Petrassi, H. M., Schumacher, A. M., Montal, M., Bandell, M. & Patapoutian, A. (2015) Chemical activation of the mechanotransduction channel Piezo1. *Elife*, 4.

Yu, H., Miao, Y., Chen, W., Qi, X., Yang, X., Pan, X., Wang, K. & Zhu, W. (2019) Expressional and functional involvement of gap junctions in aqueous humor outflow into the ocular trabecular meshwork of the anterior chamber. *Mol Vis*, 25, 255-265.

Zhu, W., Jain, A., Gramlich, O. W., Tucker, B. A., Sheffield, V. C. & Kuehn, M. H. (2017) Restoration of Aqueous Humor Outflow Following Transplantation of iPSC-Derived Trabecular Meshwork Cells in a Transgenic Mouse Model of Glaucoma. *Invest Ophthalmol Vis Sci*, 58(4), 2054-2062.